Should we point them away from the sun?

-A study in PV spectral tracking in a Scandinavian climate

Petter Stefansson

Master thesis in Energy-efficient and Environmental Buildings Faculty of Engineering | Lund University | June 2015

Abstract

Conventional photovoltaic solar tracking is commonly done by aligning the surface normal of a PV module with the direction from which direct solar irradiation is coming from. While this tracking design has proven to perform well in sunny climates, solar tracking is altogether less common in northern climates where the direct solar irradiance is weaker. In this study a radiative transfer model is used to approximate the wavelength distribution of incident solar radiation reaching Visby on the island of Gotland in Sweden during 2011 to investigate if the site specific irradiation of a northern climate in combination with different PV materials optical properties can result in circumstances where there are more productive things to track than the direct solar irradiation. The results of the study indicates that the performance of a tracking system to some extent depends on the choice of PV cell material used in the system and that the spectral response of different materials often make them achieve optimum productivity at slightly different tilt/azimuth combinations. The study concludes that a conventional tracking system in Visby during 2011 in general would generate approximately 10 kWh/m^2 less electricity compared to a theoretically optimal tracking system.

Keywords*: Solar tracking, spectral irradiance, spectral mismatch factor, radiative transfer model, PV spectral response.*

Table of content

Definitions

a-Si – Amorphous silicon. Material used in photovoltaic cells.

Absorption band – Molecule specific range of wavelengths within the electromagnetic spectra where a characteristic absorption or change in energy state takes place.

Angle of incidence – Angle between direct solar irradiance and the normal of a surface.

ASTM – American Society for Testing and Materials. Organization that creates and publishes technical standards, including standard solar spectra for PV performance ratings.

Broadband irradiance – Solar irradiance integrated across all wavelengths of an incident solar spectra.

CdTe – Cadmium Telluride. Material used in photovoltaic cells.

Declination angle – Angle between earth's celestial equator and the sun. Varies between around $\pm$ 23,45° depending on season.

GaInP – Gallium Indium Phosphide. Material used in photovoltaic cells.

Global horizontal irradiance – *S*olar radiation composed of a combination of direct and diffuse irradiance reaching a horizontal surface.

InP – Inorganic and Nanostructured Photovoltaics. Material used in photovoltaic cells.

Mono-Si – Monocrystalline Silicon. Material used in photovoltaic cells.

Multi-Si – Multicrystalline Silicon. Material used in photovoltaic cells.

SBDART – Santa Barbara DISORT Atmospheric Radiative Transfer model. Radiative transfer model developed by the University of California capable of simulating both clear and cloudy skies.

SMARTS – Simple Model of the Atmospheric Radiative Transfer of Sunshine. Radiative transfer model commonly used when simulating cloudless skies, also used to generate the G173-03 spectra.

SMHI – Swedish Meteorological and Hydrological Institute. Swedish government agency that specializes in climate monitoring and research.

SMMF – Spectral Mismatch Factor. Factor that describes the influence spectral deviations between incident and reference spectra will have on PV electricity production.

Solar altitude – Height between horizontal plane and the sun, expressed in degrees, perceived by an observer. Also called solar elevation angle.

STC – Standard Test Conditions. Standardized conditions under which photovoltaic modules are tested to enable performance comparisons between various manufacturers and materials.

Troposphere – Atmospheric layer closest to the surface of the earth containing a majority of all the atmospheres mass, water vapour, aerosol content etc.

Weighted irradiance – The product of broadband irradiance and spectral mismatch factor. Expressed in Watts per square meter but considers the underlying spectral distribution and material response properties.

Zenith angle – Angle between sun and the normal of a horizontal surface.

ZnO/CIGS – Copper Indium Gallium Selenide with Zinc Oxide. Material used in photovoltaic cells.

1 Introduction

1.1 Background

When simulating the expected annual PV electricity production using standard *Typical Meteorological Year, TMY,* weather files, the solar irradiance only comes expressed as *broadband irradiance* [1], which is irradiance integrated across all wavelengths of the electromagnetic spectrum, but is in practice generally limited to the wavelength sensitivity range of the irradiation measuring instruments [2]. This *broadband irradiance* is then normally assumed by most calculation approaches and simulation software to be composed of the same underlying wavelength distribution as was present during *Standard Test Conditions, STC.* The *STC* are standardized specific conditions used when determining the performance of photovoltaic cells and they dictate an ambient temperature of $25°C$ and an incident irradiance of $1000\ W/m^2$ distributed according to a AM1.5G reference spectra [3] such as the standardized *ASTM G173-03* spectra [4]. This reference spectra has been designed to represent a situation when the *air mass* is 1.5, meaning that the direct solar irradiance has to pass through 1.5 times more atmosphere compared to the shortest possible atmospheric path at sea level. While this very well could be a realistic estimation of a normal atmospheric distance the solar radiation has to travel through during many days of a year in a warm southern location, in northern locations such as Scandinavia, the *solar altitude* fluctuates greatly throughout a year and during big parts of autumn, spring and especially winter the *air mass* can as a consequence often be far greater than 1.5. A longer atmospheric path enables more absorption and scattering to take place before the irradiation reaches the earth's surface and therefore the spectral distribution of incident sunlight may potentially have altered in a way that makes it quite different from the $AM1.5$ reference spectra, which could influence the electricity production.

Since the $AM1.5$ reference spectra represents only one moment in time, which has been chosen to represent *"reasonable cloudless atmospheric conditions favorable for photovoltaic (PV) energy production"* [5] all atmospheric constituents such as water vapour, ozone, carbon dioxide, aerosols etc. are assumed to be constant throughout the whole year in any energy simulation approach based solely on information about PV-panels that have been acquired during *Standard Test Conditions*. In reality none of the atmospheric constituent remain at a perfectly constant concentration during the course of a year and some chemicals exhibit clear seasonal variations which has the potential to alter the absorption and scattering properties of the atmosphere, and since each PV-material uses a specific segment of the solar spectra to generate electric current, any change in spectral distribution of incident light can influence the PV performance in ways that are not necessarily accounted for in the *broadband irradiance* [6]. Furthermore, the reference spectra represents a cloudless sky, so any calculation approach that only uses PV-performance data obtained under *STC* in combination with *broadband irradiance* from a weather file is more or less treating the whole year as cloud free and is only accounting for the effects of clouds by a spectrally uniform decrease in irradiance. In reality clouds influence the available solar radiation more than anything on a site except for the day-night cycle [4] and their influence cannot always be considered completely even throughout the electromagnetic spectra. Seen on an annual basis it is for these reasons not even a question of if the incident solar spectra of a site will differ from the

reference spectra or not from time to time, but how much and in what way – is the site specific spectral divergence favorable for photovoltaic electricity production or unfavorable?

This question can be answered by calculating a parameter known as the *spectral mismatch factor* [7] which considers the wavelength dependent *spectral response* of a semiconducting material used in photovoltaic applications along with information about the present incident solar spectra and a reference spectra to determine how well suited the wavelength distribution of the incident sunlight is compared to the reference spectra for conversion to electric current.

This study will investigate the effects of the spectral mismatch in solar tracking device applications. Conventionally, solar tracking is done by continuously directing a PV panel towards the sun so that the angle between the surface normal of the panel and the sun is minimized. When estimating the annual electricity yield from a PV system with solar tracking, PV simulation software such as for example *System Advisor Model*, developed by the *National Renewable Energy Laboratory*, *NREL*, assumes that a continuous minimization of the incidence angle between the PV module and incident direct solar irradiation is what the user wants when enabling solar tracking in a simulation and calculates the energy production accordingly. This study will consider the spectral distribution and intensity of sunlight coming from all directions surrounding a PV module during a year together with the spectral responsiveness of specific cell materials to determine whether pointing our panels directly towards the sun is indeed the best thing to do or if there are other directions more favorable for PV electricity production that up until now might have been overlooked.

1.2 Methodology and study approach

Since spectrally resolved solar irradiance is not something that usually is continuously measured by weather stations, anyone who wishes to obtain a site specific solar spectra for a given time and location has to approximate it using a *radiative transfer model* in combination with knowledge about the suns position and measured data of the atmospheric constituents above the simulated site. *Radiative transfer models*, also known as *radiative transfer codes*, are software products that mathematically predicts the attenuation of electromagnetic radiation due to absorption and scattering processes caused by chemicals and particles as it travels through the atmosphere. With the assumption that the extraterrestrial solar spectra remains constant over time it then becomes possible to approximate the wavelength distribution of sunlight reaching the earth's surface simply by knowing the constituents that makes up the atmosphere.

A large number of *radiative transfer models* exists, many of which are so called clear-sky models, which are only capable of simulating radiative transfer without the presence of clouds. Because of its capability to simulate both clear and cloudy skies [8], the *Santa Barbara DISORT Atmospheric Radiative Transfer model*, *SBDART*, developed by the *University of California* in Santa Barbara will be used in this study to compute the spectral distribution of the solar irradiation that reached a horizontal surface on a minute-by-minute basis during 2011. The spectral irradiance will then be used to assess how various panel orientations and PV materials are effected by the incident irradiation and if situations occur during a year that are spectrally favorable for electricity production, and which are potentially missed when only assessing the situation through *broadband irradiance*, that are worth considering in a solar tracking context. The site that will be simulated in this study is located at the *Swedish*

Meteorological and Hydrological Institute's, *SMHI*'s, weather station in Visby on the island of Gotland in south-eastern Sweden, lat. 57.67° long. 18.35°.

By using a combination of satellite data and data measured by the weather station on the site itself, a parameterization of the primary factors that influenced the attenuation of solar irradiance over Gotland during 2011 will be created and fed as input data into the *radiative transfer model SBDART* to obtain spectrally resolved irradiation. The atmospheric features that predominantly influence radiation attenuation are clouds, air mass, water vapour content, ozone content, carbon dioxide content and aerosol properties [9][10]. It is also possible for radiation to reflect off the surface of the earth and interact with clouds and the atmosphere a second time, to be able to account for this it is also necessary to parameterize the earth's reflective properties through an *albedo* value. It should be noted that the atmosphere also contains many other molecules and chemical compounds such as nitrogen, oxygen, methane, carbon monoxide, nitric acid etc. [11] many of which can also be quantified and used as input in *radiative transfer models,* the content variation of these constituents is however generally considered to not influence the spectral distribution enough for it to be necessary to accurately model them for PV-applications. Atmospheric constituents that has not explicitly been assigned a Gotland related value during the radiative transfer simulation will assume the concentration value specified in the standardized atmospheric profile *U.S. Standard Atmosphere, 1962*.

The *radiative transfer model* will produce an approximation of the spectrally resolved irradiation reaching Visby during 2011 expressed on a horizontal surface with a direct and global component. To study the spectral effects in terms of photovoltaic tracking devices, the spectrally resolved horizontal irradiation will be recalculated to represent every combination of panel tilt and azimuth that can occur during the year, which then will be used in conjunction with the *ASTM G173-03* reference spectra to determine a *spectral mismatch factor* for each of the corresponding tilt/azimuth combinations. The *spectral mismatch factor* of each panel orientation will then be combined with the *broadband irradiance* measured by the weather station on the site to generate a *weighted irradiance* for each of the panel orientations which accounts for spectral divergences and which will prove if there are more productive directions to point a PV-panel at other than the sun, and if so – what are they and how much more electricity could be produced by continuously directing the PV-panel in a spectrally optimal way? Since PV modules can be constructed from a variety of different materials with different spectral sensitivities, some potentially more favored by a Scandinavian climate than others, eight different semiconducting materials will be assessed in the study.

The sun outputs a continuous spectra covering a very wide range of frequencies, as will be shown in chapter 4.1, PV materials are only responsive to wavelengths up to about $1300\ nm$, and since the spectral intensity of solar irradiation gets weaker and weaker as one moves further in to the infrared region, this study will not include wavelengths beyond $2500\ nm$ and will only focus on the $280 - 2500\ nm$ region to speed up the required calculation time. The study is structured so that it starts with a brief introduction to the solar spectra, which is then followed by an overview of the collected atmospheric data above Visby during 2011 and the potential effects each atmospheric compound can have on the spectral distribution of sunlight passing through the atmosphere. Afterwards the calculation sequence that results in the *weighted irradiance* is explained and the results of the study are presented and discussed.

2 The solar spectra

2.1 Thermal radiation and solar energy

All matter with a temperature above absolute zero emits radiation. The spectral distribution and peak wavelength of the radiation depends on the temperature of the body. In the case of ideal black bodies, bodies that absorbs all incoming radiation and remains at thermal equilibrium with its surroundings, the spectral distribution and intensity of the emitted radiation can be described using Planck's radiation law:

$$F(\lambda) = \frac{2 \cdot \pi \cdot h \cdot c^2}{\lambda^5 \cdot (e^{\frac{h \cdot c}{k \cdot \lambda \cdot T}} - 1)} \quad (\mathrm{W} \cdot m^{-2} \cdot \mu m^{-1}) \tag{1}$$

where λ is the wavelength of the radiation, h is the Plank constant $6.626 \cdot 10^{-34}$ Js, c is the speed of light $2.998 \cdot 10^{8}\ m/s$, T is the absolute temperature of the body, k is the Boltzmann constant $1.381 \cdot 10^{-23}\ J/K$ and F is the spectral emittance of the body. In reality however, no bodies behave completely like perfect ideal blackbodies and therefore modelling the emitted radiation of real life objects with Planck's radiation law will likely never yield a completely realistic result. This is also true for astronomical objects such as our sun, however, modelling the emitted radiation of a star with Planck's radiation law generally results in a reasonably accurate approximation of its emitted radiation [12].

The warmer a radiating object is, the more shifted towards shorter wavelengths the point of maximum intensity becomes. This is why a burning matchstick will appear mostly red/yellow while the flame of a warmer blowtorch is perceived as blue. The exact spectral position at which the emitted radiation reaches its maximum intensity is a direct consequence of its absolute temperature and is described by Wien's displacement law:

$$\lambda_{\max} = \frac{b}{T} \quad (m) \tag{2}$$

where λ_{max} is the peak wavelength, T is the absolute temperature of the body and b is Wien's displacement constant $2.897\ 7721 \cdot 10^{-3} m \cdot K$. This means for example that the spectral emissions of a human body with a temperature of $37°C$ ($310.15\ K$) approximately peaks at a wavelength of about 9342 nm, far into the infrared region and well outside the visual part of the spectrum. The solar energy we receive on earth originates from the center of the sun, where hydrogen atoms collide at high speeds and immense pressure leading to a series of fusion reactions taking place which ultimately results in the conversion of hydrogen atoms into helium. The continuous fusion processes taking place at the center of the sun causes temperatures as high as $15\ 710\ 000\ K$ [13], luckily for us on earth, this temperature does not directly give rise to the solar spectra we are reached by. The emitted thermal radiation reaching us from the sun comes from the suns outer surface, its *photosphere*, where the temperature is significantly lower and the mean temperature is around $5760\ K$. Figure 1 shows the electromagnetic spectrums caused by thermal radiation calculated with equation 1

for three different absolute temperatures together with the corresponding peak wavelength according to equation 2.

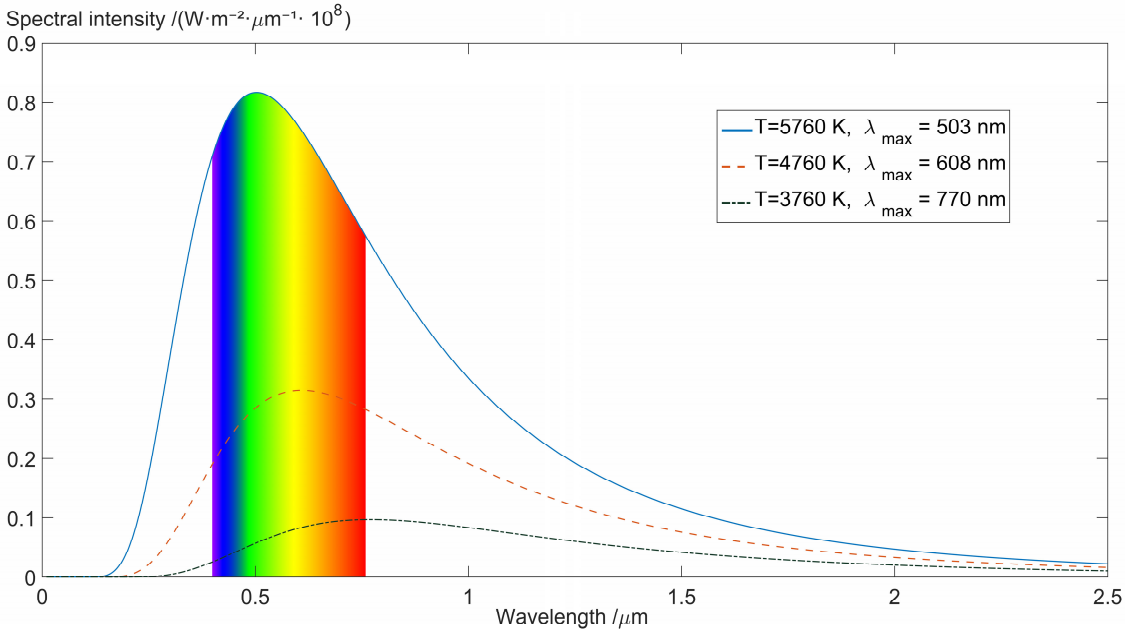

Figure 1. Black body radiation according to Plank's radiation law calculated for three different temperatures.

As can be seen from the $5760\ K$ curve in Figure 1, the blackbody radiation emitted by the suns *photosphere* is most intense in the visual part of the spectrum and peaks around the $503\ nm$ region, which corresponds to a color perceived as green by humans. Once an emitted photon has left the *photosphere* of the sun there is very little matter standing in its way of reaching the top of the earth's atmosphere [14], therefore, the spectral distribution of the light remains virtually unchanged from the time it left the sun to the time it reaches the top of earth's atmosphere. Due to a layer of gas surrounding the sun, known as the suns *chromosphere* [12], some molecular interactions triggering radiation absorption does however occur already in space, which results in the solar spectra observed at the top of the earth's atmosphere, also known as the $AM0$ spectra, not appearing as smooth and ideal as the blackbody spectra shown in Figure 1.

The radiation from the sun is emitted isotopically in all directions into space, and consequently, even though the intensity of the radiation isn't diminished as it travels, the power density of the sunlight is reduced with an increased distance from the source. As the solar irradiation travels further out into space its power is spread over a bigger and bigger spherical surface area and is reduced according to the inverse-square law [13], meaning that the power density of the sun is inversely proportional to the squared distance from the source.

The earth orbits around the sun in a slightly elliptical path, meaning that the distance between the sun and the earth varies during an annual cycle. For simplicity the distance between the sun and the earth is however usually said to be roughly $149\ 597\ 870\ 700\ m$, defined as one *astronomical unit*, AU [15]. Considering that the sun is an isotropic emitter with a radius of

about $6.960 \cdot 10^8\ m$ [16], it then becomes possible to construct a sphere around the sun with a radius of $1\ AU$ to estimate what the power density of the integrated $5760\ K$ blackbody irradiance seen in Figure 1 will be when it reaches earth with the following formula:

$$G_{AM0} = \frac{P_{sun} \cdot 4\pi \cdot r_{sun}^2}{4\pi \cdot d_{sun-earth}^2} = \frac{\int \mathrm{F}_{5760\mathrm{K}}(\lambda)\,\mathrm{d}\lambda \cdot 4\pi \cdot (6.960 \cdot 10^8)^2}{4\pi \cdot 149\,597\,870\,700^2} \approx 1360 \quad (\mathrm{W} \cdot m^{-2}) \tag{3}$$

where P_{sun} represents the power emitted by the sun across all wavelengths, r_{sun} is the radius of the sun and $d_{sun-earth}$ is the distance between the sun and the earth. The resulting value seen in equation 3, roughly $1\,360\ W/m^2$, corresponds to the *broadband irradiance* impinging on the top of the earth's atmosphere at normal incidence. In reality however, the sun doesn't radiate exactly like an ideal blackbody, the earth-sun distance doesn't remain at a constant $1\ AU$ and the emitted energy from the sun isn't entirely constant over time. Therefore, the *broadband irradiance* we receive at the top of the atmosphere doesn't remain at a fixed constant value but tends to fluctuate between about 1363 and $1369\ W/m^2$. For simplicity, the *broadband irradiance* received at normal incidence at the top of earth's atmosphere with an earth-sun distance of $1\ AU$ is typically referred to as the *solar constant*, which has been defined as $1366.1\ W/m^2$. In photovoltaic applications, using the *solar constant* to describe the intensity of energy reaching the top of the atmosphere is usually considered adequate and deviations from the *solar constant* are typically neglected [17]. Figure 2 shows the satellite measured *broadband irradiance* at the top of earth's atmosphere between 1982 to 2015 together with the defined *solar constant*.

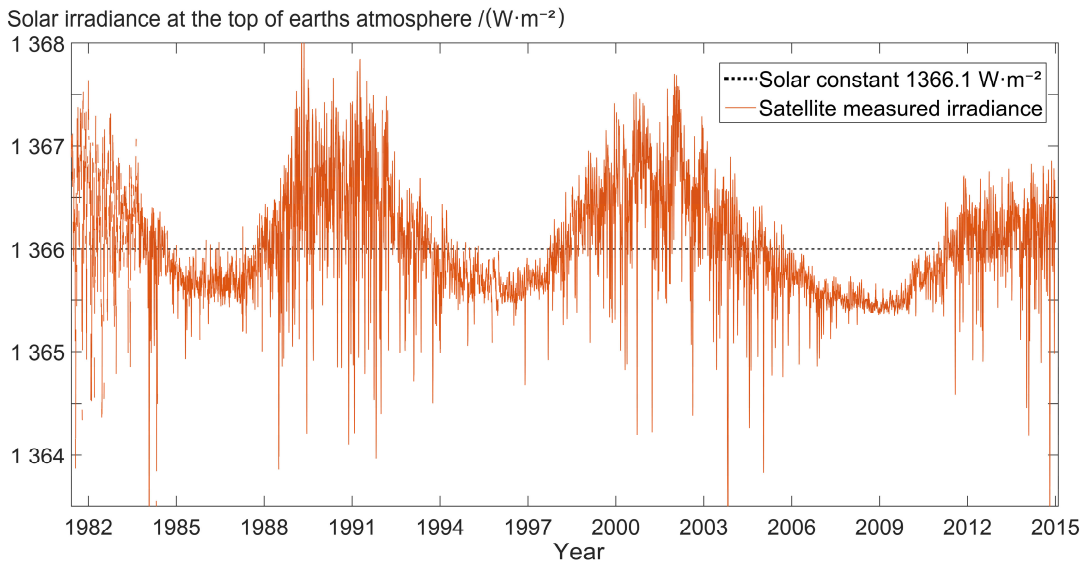

Figure 2. Satellite observations of the daily mean solar irradiance intensity at the top of the earth's atmosphere between 1982 and 2015 compared to the solar constant. Data from [18].

It is easy to intuitively assume that the theoretical maximum value of irradiation making it through the atmosphere and reaching the surface of the earth is limited by the *solar constant* and that the intensity of terrestrial radiation never can surpass the extraterrestrial radiation.

And while this is generally the case, due to a phenomena called *overirradiance*, occurring when thin clouds form a circle around the sun disk acting like a focusing lens, some field studies have measured short bursts of naturally occurring terrestrial irradiation as high as 1800 W/m^2 [19], paradoxically this means that the "sunniest" days are days that are partially cloudy.

2.2 Extraterrestrial and terrestrial standard spectrum

As seen in Figure 2 the intensity of the solar energy reaching the top of earth's atmosphere, also known as the extraterrestrial solar energy, isn't entirely constant over time. The atmospheric constituents that makes up the earth's atmosphere also vary with time and geographic location which leads to a wide variety of solar energy distributions occurring in the natural environment, both in terms of intensity and spectral distribution. To be able to compare the performance of various spectrally sensitive products, including photovoltaic cells, several standardized solar spectrums have been developed over the years, both terrestrial and extraterrestrial ones. Extraterrestrial reference solar spectrums are commonly defined so that their integrated spectral irradiance, i.e. the *broadband irradiance*, roughly matches the *solar constant* and they are primarily used by aerospace industries. It is however also necessary in earth based photovoltaic applications to have an extraterrestrial reference spectrum defined since this is used as a starting point when determining the wavelength distribution of the terrestrial spectra. With a defined extraterrestrial solar spectra any desired terrestrial spectra can be generated using a *radiative transfer model* together with information about the atmospheric constituents at hand, which is also how the standardized *ASTM G173-03* terrestrial $AM1.5$ solar spectra was established [5]. The *ASTM* document describing their $AM1.5$ reference solar spectra contains detailed information about the concentration of different atmospheric compounds and how to enter them into the *radiative transfer model Simple Model of the Atmospheric Radiative Transfer of Sunshine*, *SMARTS*, in order to generate an exact replica of the *ASTM G173-03* reference spectra. A *SMARTS* simulated *ASTM G173-03* reference spectra can be seen in Figure 3 together with the *ASTM E-490-00* standardized $AM0$ extraterrestrial spectra.

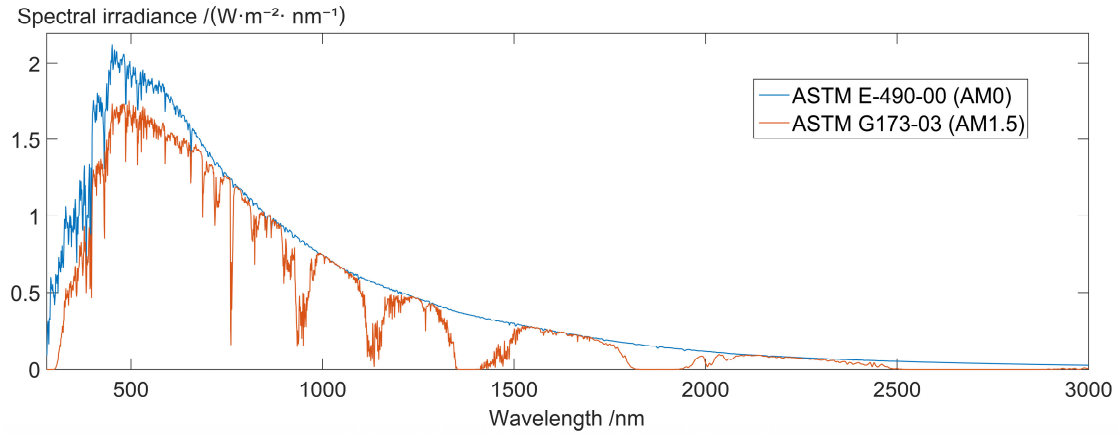

Figure 3. Standard extraterrestrial (ASTM E490) and terrestrial (ASTM G173) spectrum in the 280-3000 nm region.

The atmospheric data used to model the *ASTM G173* reference spectra does not originate from one site and time specific measurement, instead it is derived from several different weather stations in the U.S. that were considered to represent conditions favorable for PV energy production [5]. The modeled atmosphere used to generate the *G173-03* spectra has also been chosen so that the integrated intensity of the resulting spectra in the $280 - 4000\ nm$ range becomes $1\ kWh/m^2$ and thereby matches the irradiance intensity requirement dictated by the *Standard Test Conditions* for PV performance rating applications without the need for any amplitude adjustment.

3 Atmospheric variations in Visby

This chapter provides an overview and an explanation of the data used as input to the *radiative transfer model* used in this study to simulate the spectrally resolved irradiance reaching Visby during 2011.

3.1 Air mass

The *optical air mass*, also known as the *atmospheric length,* usually abbreviated *AM,* is a factor describing how much longer direct sunlight has to traverse through the earth's atmosphere to reach the surface of the earth compared to a situation at zero degrees *zenith angle* at sea level, which is defined as $AM1$ [20]. As illustrated in Figure 4, it is easy to see that the smaller the angle between the horizon and the sun is, the greater the path through the atmosphere will be and consequently the larger the *air mass* will be.

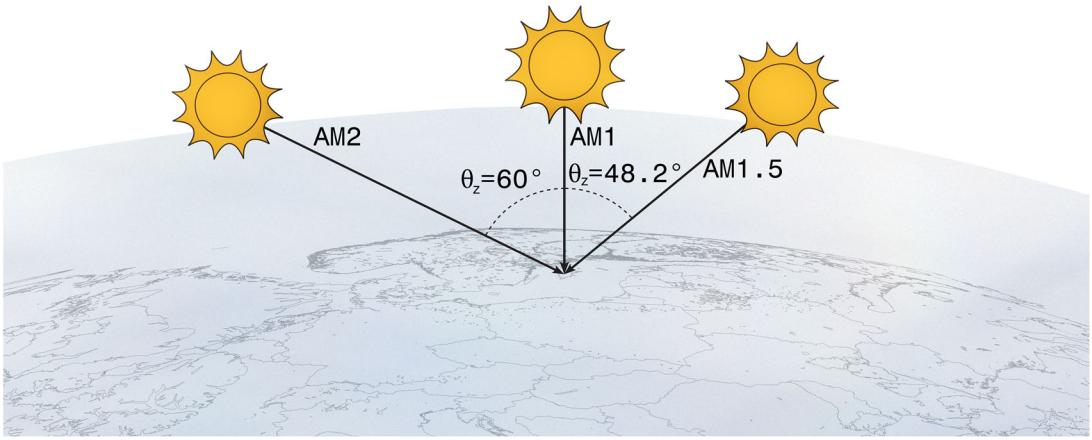

Figure 4. Illustration of air mass increasing with solar zenith angle.

While the *air mass* isn't in itself an atmospheric property causing any characteristic absorption per se, it does play an important role in radiation attenuation since it regulates how long the path will be where light interacts with all other atmospheric components. The *air mass* can be calculated with a known solar *zenith angle* according to equation 4:

$$AM = \frac{1}{\cos(\theta_z) + 0.50572 \cdot (96.07995 - \theta_z)^{-1.6364}} \tag{4}$$

where θ_z represents the solar *zenith angle* and the constant numeric values accounts for the curvature of the earth [21]. In northern locations such as Scandinavia, the solar *elevation angle*, to which the *zenith angle* is directly linked, fluctuates greatly during the course of a year, and consequently, so does the *air mass*. Figure 5 illustrates the lowest *air mass* notations above Visby during January to July 2011 calculated with equation 4 together with a line representing $AM1.5$.

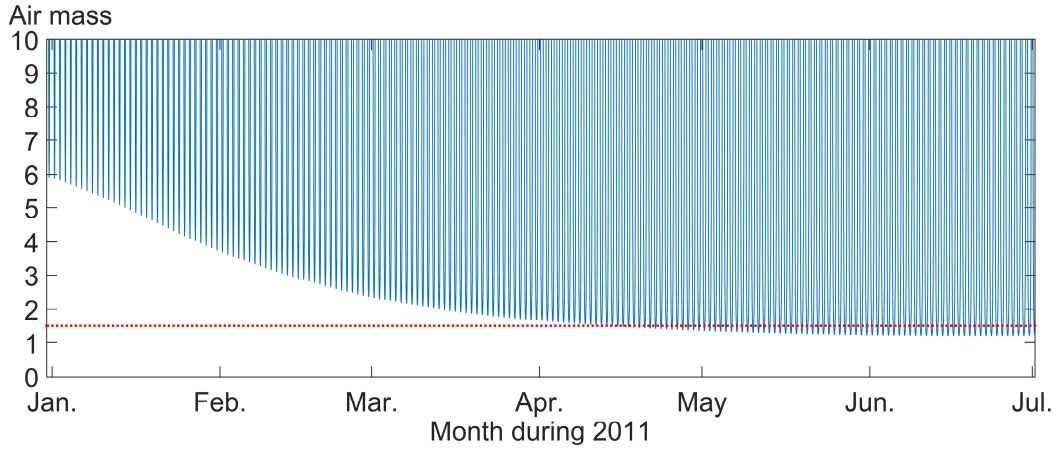

Figure 5. Blue line representing daily minimum atmospheric air mass variation from January to July over Visby together with red horizontal line marking AM1.5.

As can be seen in Figure 5, an *air mass* equal to or smaller than 1.5, which is assumed during *Standard Test Conditions*, is a rare sight in Visby and should almost be considered an annual minimum rather than a representative average.

3.2 Ozone

Data collected by the *Ozone Monitoring Instrument*, *OMI*, onboard *NASA*'s *Aura* satellite was used to gather input data for the radiative transfer simulation in this study about the daily variations in atmospheric ozone content over Visby during 2011. Atmospheric ozone is commonly measured in *Dobson units*, which describes the density of a trace gas in a column of the earth's atmosphere. More specifically, one *Dobson unit, DU*, is defined as the number of O_3 molecules it would take at a temperature of $0°C$ at sea level to create a $0.01\ mm$ thick layer of ozone [22]. On average, the ozone layer above earth is around $300\ DU$, meaning that if brought down sea level at $0°C$ it would only be around $3\ mm$ thick. The scarcity of atmospheric ozone in combination with its proneness to interaction with other chemicals makes it vulnerable to man-made chemical emissions. Chlorofluorocarbons, CFCs, which are now banned, were widely used during many years as solvents and refrigerants and it wasn't until the 1970's when researchers started to investigate the effect chemicals had on atmospheric ozone that it was realized that CFCs and other chemicals were causing a large scale ozone depletion, giving rise to the famous concept of the "ozone hole" over Antarctica

which can still be seen today but technically isn't a real hole but rather an area with a lower than average ozone concentration [23].

Despite the atmospheric content of ozone being very low compared to other atmospheric constituents, ozone plays an important role when it comes to absorbing certain wavelengths of solar radiation. Like most elements ozone absorbs radiation in a number of different regions in the electromagnetic spectrum, but most significant are the so called *Hartley bands* and *Huggins bands* [24], which intensely absorbs short wave radiation in the $200 - 300\ nm$ and $310 - 360\ nm$ regions respectively. This absorption is crucial for the well-being of life on earth which can be illustrated by the relationship between the energy of a photon and its wavelength which is given by:

$$E(\lambda) = \frac{h \cdot c}{\lambda} \quad \text{(J)} \tag{5}$$

where h is the Plank constant $6.626 \cdot 10^{-34}$ Js, c is the speed of light $2.998 \cdot 10^{8}\ m/s$ and λ is the wavelength of the radiation. As can be seen from equation 5 this means that the shorter the wavelength of the radiation is the more energetic its photons are. The radiation absorbed in ozone's *Hartley* and *Huggins bands* is in the UV-region of the spectrum and is so energetic that when hitting organisms or materials it can dissociate molecules within them [25], potentially causing damage, degradation or cancer.

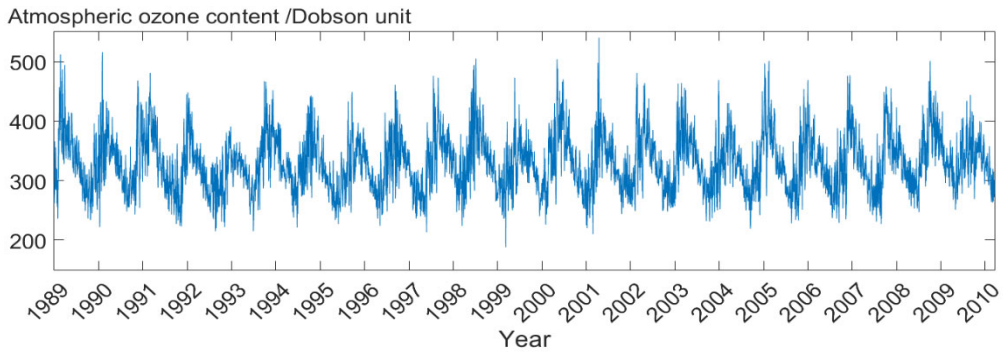

Figure 6. Historic variation of atmospheric ozone content over Visby from 1989-2010. Data from [26].

As can be seen in Figure 6, illustrating the measured long term ozone variations above Visby, the atmospheric ozone content appears to follow an extremely repetitive annual pattern, with each year being almost an exact replication of the previous one. Before satellite measured data of ozone content became readily available the atmospheric ozone variations used in *radiative transfer models* were often not measured at all, but calculated using an empirically developed equation known as *Van Heuklon's ozone model* [27] which for northern Europe is described as:

$$O_3 = 235 + (150 + 40 \cdot \sin(0.9865 \cdot (E - 30)) + 20 \cdot \sin(3 \cdot (\lambda + 20)) \cdot \sin^2(1.28 \cdot \varphi))$$

$$(matm \cdot cm) \tag{6}$$

where E is day number of the year, λ is the longitude of the site and φ is the latitude. As can be seen in Figure 7 showing a comparison between satellite measured and modelled daily ozone during 2011 over Visby, *Heuklon's model* does a reasonably good job at capturing the shape of the seasonal ozone trend. But due to decreasing ozone levels during the 1980-1990s the model tends to overestimate todays ozone values and is therefore nowadays often considered to not provide an acceptable accuracy anymore [27] and was therefore not used to generate input data for the *radiative transfer model* in this study, which instead relies on the satellite data seen in Figure 7.

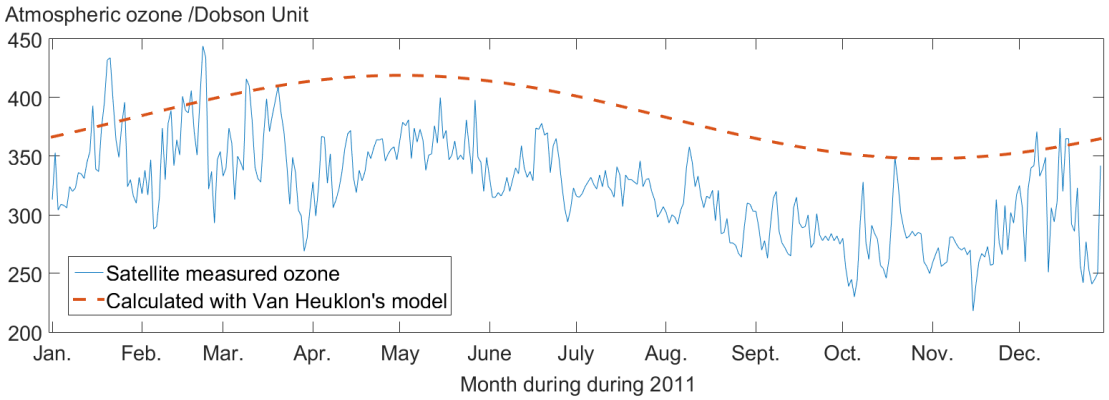

Figure 7. Atmospheric ozone variation above Visby during 2011 with satellite observations and calculated estimations with Van Heuklon's model. Satellite data from [26].

Apart from the UV-absorption in the *Hartley* and *Huggins bands*, ozone also absorbs radiation in the visual part of the spectra. The simulated spectral impact of an increasing ozone content can be seen in Figure 8.

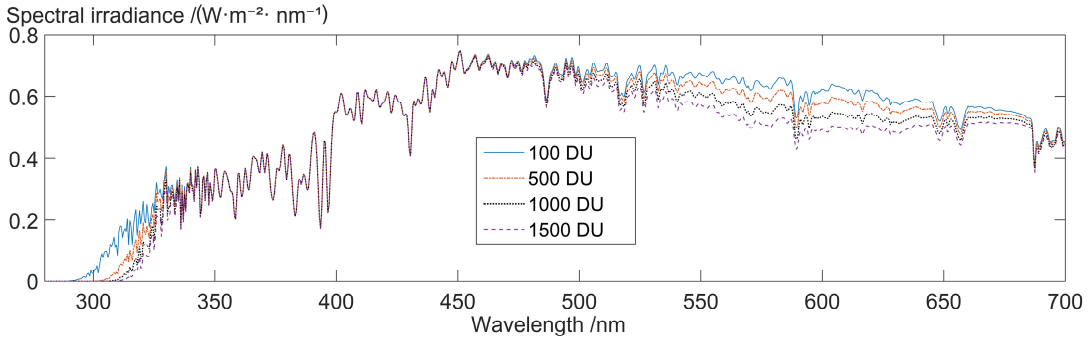

Figure 8. SBDART simulated spectral effects of various atmospheric ozone contents in the 280-700 nm region.

3.3 Carbon dioxide

The concentration of carbon dioxide over Visby during 2011 used as input data to the *radiative transfer model* in this study was measured by the *atmospheric infrared sounder*, *AIRS*, and its companion instrument the *advanced microwave sounding unit AMSU*, mounted on the *NASA*'s *Aqua* satellite. The CO_2 observations used in this study have a temporal

resolution of 24 hours. The carbon dioxide concentration during 2011 varied between 381 PPM, which occurred on the 30th May and 397 PPM which was measured on the 25th of October. As can be seen in Figure 9, during the course of 2011 the CO_2 concentration doesn't appear to exhibit any clear seasonal behavior but rather fluctuates in a seemingly random fashion on and around the 390 PPM mark.

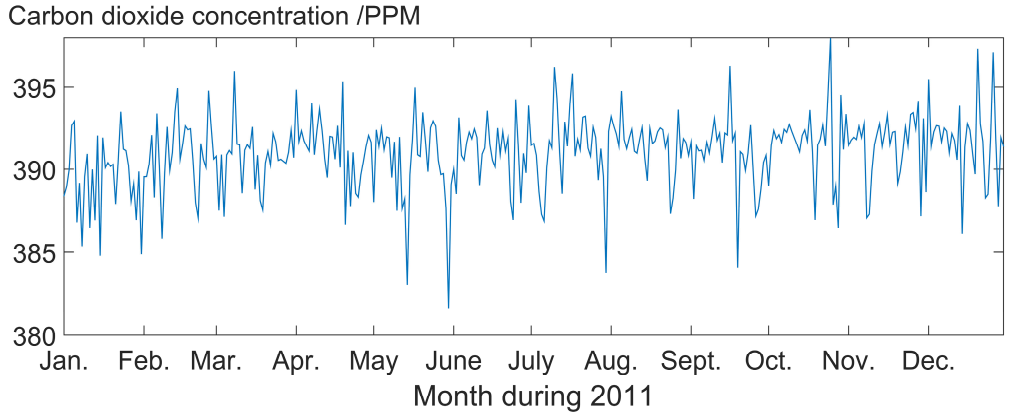

Figure 9. Carbon dioxide concentration in the atmosphere above Visby during 2011. Data from [28].

It can however be noted that the last measured value during 2011 is slightly higher than the first measured value, which could be part of a more long term trend in globally increasing carbon dioxide concentrations.

The effects CO_2 has on the solar irradiations spectral distribution is confined to wavelengths beyond the visual part of the spectrum. Within the region of interest of this study, $280 - 2500\ nm$, there are two main places where attenuation due to carbon dioxide occurs. These are, as shown in Figure 10, the $1530 - 1680\ nm$ and $1990 - 2120\ nm$ regions.

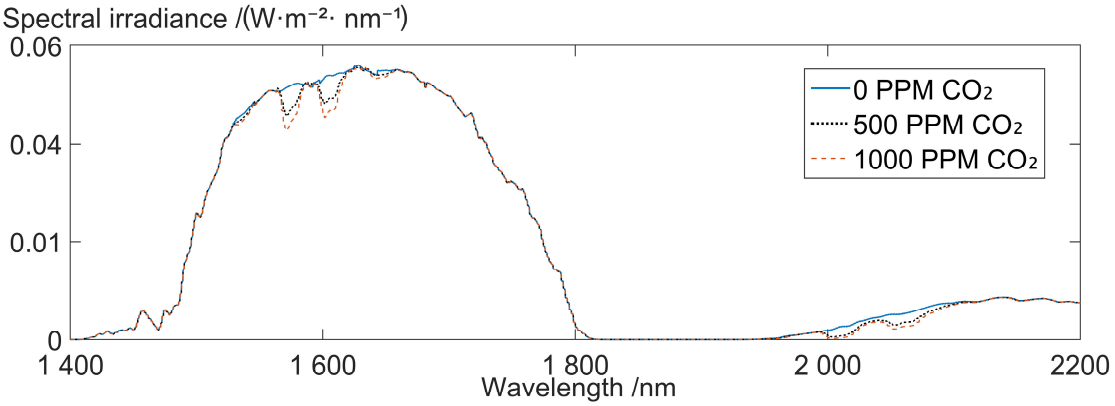

Figure 10. SBDART simulated spectral effects of various carbon dioxide concentrations in the 1400-2000 nm region.

3.4 Water vapour

Data collected by the *Advanced TIROS Operational Vertical Sounder, ATOVS*, provided by the *Satellite Application Facility on Climate Monitoring, CM SAF*, was used to determine the water vapour content in the atmosphere above Visby during 2011. To quantify the amount of water vapour in the atmosphere at any given time and location, the concept of *vertically integrated water vapour* is often used which is defined as the total mass, expressed in for example $grams$, of all water molecules within a given area, for example 1 cm^2, stretched as a column from the bottom of the earth to the top of the atmosphere, thereby making the unit g/cm^2 [29].

The water vapour content of the atmosphere is often closely linked with air temperature. Since the water amount that can be suspended in a volume of air increases with temperature, the lower the temperature of the air is the less water content is required to fully saturate it, therefore the air temperature is often limiting the amount of vapour the air can hold. It is however physically possible for the water vapour to exceed the saturation level set by temperature and air pressure and go into a state known as supersaturation [11], where the relative humidity is above 100%. But this phenomena only occurs in rare cases when the air is so clean that the water molecules are unable to find anything to condensate on.

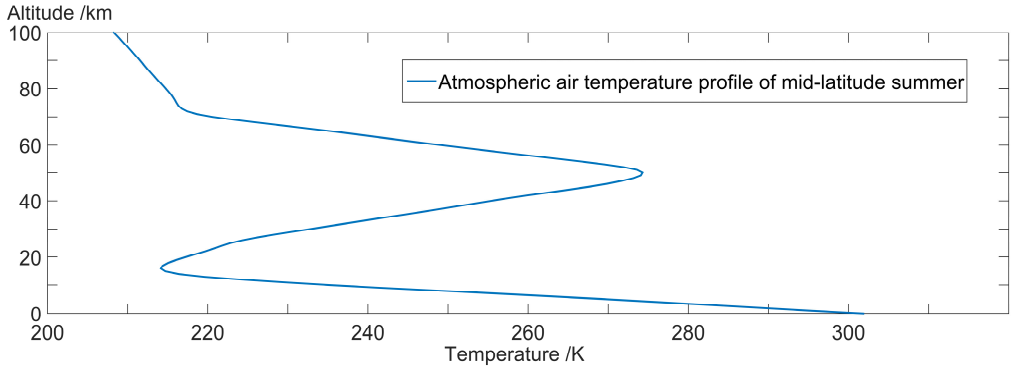

Figure 11. Air temperature as a function of altitude in one of the standard atmospheric profiles in SBDART representing a mid-latitude summer day.

The atmospheric air temperature, as illustrated in Figure 11, tends to drop rapidly from the earth's surface to the top of the *troposphere*, which is the atmospheric layer closest to the earth, at an altitude of around 20 km and then fluctuates from warmer to cooler in the different atmospheric layers above. Since water vapour originates from evaporation at sea level it is generally difficult for water vapour to overcome the barrier of cold air at the top of the *troposphere* and rise to greater altitudes without condensing or forming clouds and therefore almost all, approximately 99% [11], of the atmospheres water content is confined to the *troposphere.*

This means that a close link between the observed air temperature at surface altitude and the *vertically integrated water vapour* content of the atmosphere is to be expected. Figure 12 shows satellite measurements of how the atmospheric water vapour amount varied on a daily

basis over Visby during 2011 together with ambient air temperature readings measured every minute at *SMHI*'s weather station in Visby.

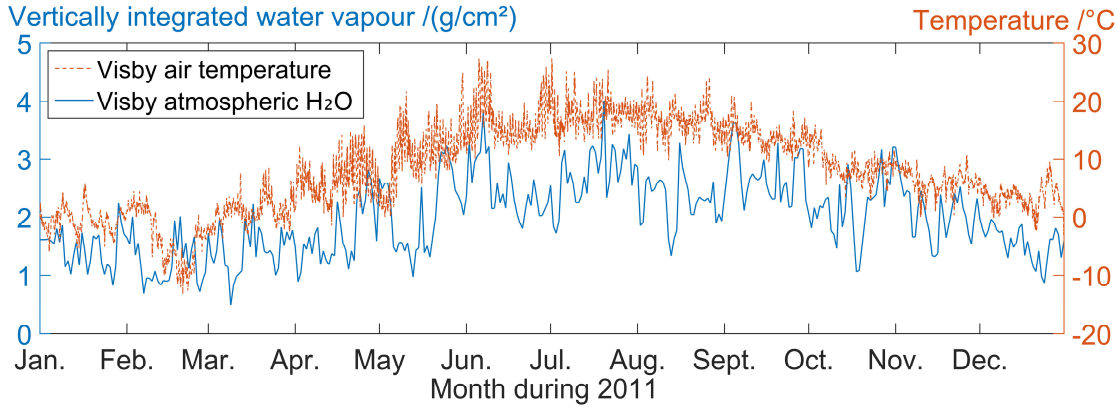

Figure 12. Satellite measured atmospheric water vapour content and air temperature at surface level in Visby during 2011. Satellite data from [30], weather station data from Thomas Carlund at SMHI.

Of all the atmospheric constituents included in the study, water vapour has by far the biggest potential to change the spectral distribution of the impinging solar irradiation. Its absorption bands stretches across large parts of the spectra with an especially strong absorption throughout the infrared region. Water vapour is typically responsible for about 70% of all absorption that takes place in the atmosphere [31] and without any water vapour in the atmosphere the earth would suffer an everlasting ice-age [32]. Water vapour is also an atmospheric component that vary a lot depending on geographic location, a column of air above a tropical rainforest can contain many times that of an identical column near the poles. Figure 13 shows the simulated spectral absorption effects of an increasing the water vapour content in the atmosphere.

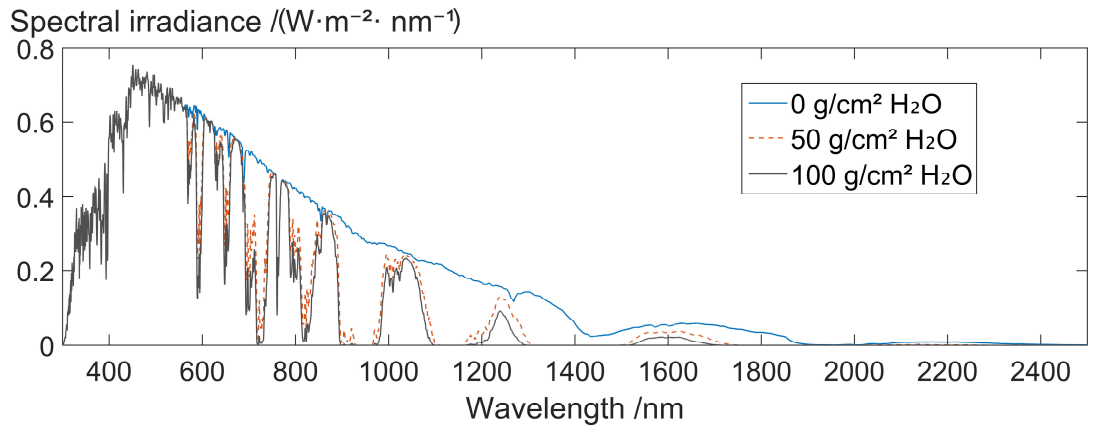

Figure 13. Simulated spectral effects of an increasing integrated water vapour content in the 300-2500 nm region.

3.5 Aerosols

Aerosols are particles suspended in the air and can practically consist of any type of substance such as for example dust, spores, minerals, bacteria, soot or pollen from plants [11]. To quantify the effects airborne particles have on solar radiation in *radiative transfer models*, aerosol content is calculated into a parameter referred to as *Aerosol Optical Thickness* or *Aerosol Optical Depth* [33]. The *Aerosol Optical Depth*, *AOD*, is defined as the vertical integration of another aerosol parameter called the *Aerosol light extinction coefficient*, which for a specific wavelength is described as a mathematical function of particle size, mass concentration and chemical composition [34]. Simply put, the higher the *AOD* is, the harder it is for light of the specified wavelength to transmit through the atmosphere. Fortunately the *AOD* is not something that every user of *radiative transfer models* individually has to derive from the *light extinction coefficient* since the required computations behind it are often already performed by the weather data provider. The *AOD* data used as input in the *radiative transfer model* in this study was measured by *SMHI*'s weather station in Visby and was provided in a minute-by-minute temporal resolution during every day of 2011. According to Thomas Carlund, the meteorologist at *SMHI* who provided the *Aerosol Optical Depth* at 500 *nm* data used in this study, aerosol measurements can only be carried out accurately at times when the sky is cloud-free. This is why vertical gaps can be seen in some parts of the *AOD* data measured in Visby during 2011 which can be seen in Figure 14. When performing the radiative transfer calculations with *SBDART* in this study, any missing *AOD* data was assigned to be the same as the last previous known valid data point, and assumed constant until a time step with another valid data point occurs.

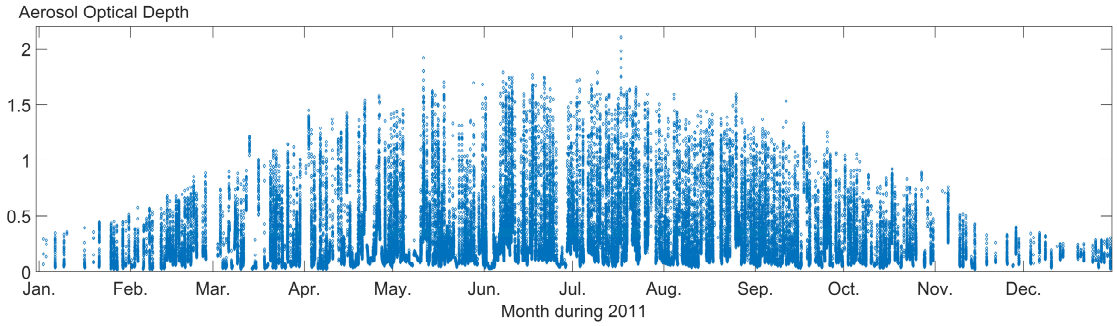

Figure 14. Minute-by-minute variation in aerosol optical depth in Visby during 2011. Data provided by Thomas Carlund at SMHI.

In terms of seasonal variation, few atmospheric constituents display such a clear pattern as *AOD*, with a maximum occurring in spring/summer and a minimum during winter. The main driving forces behind this pattern are temperature and humidity; as the soil gets warmer and dryer more dust and fine particles gets released into the air and gets picked up by the wind and when spring comes along plants starts producing pollen which gets released into the air [35]. Furthermore, as the temperature increases with season, so does evaporation from the ocean and when water droplets from the sea evaporates the salt contained in the water can be left suspended in the air, forming what's known as *maritime aerosols*. It has been estimated

that the ocean each year releases somewhere in between $1-10$ trillion kg [11] of aerosols into the air in the form of sea salts and algae.

The radiation absorption potential of aerosol content generally decreases with increasing wavelength [36]. Figure 15 shows the simulated spectral effects of an increasing *AOD*.

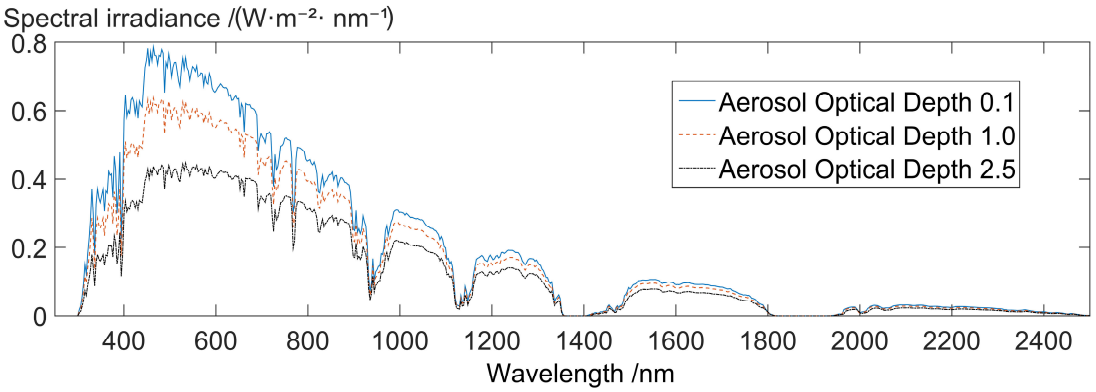

Figure 15. Simulated spectral impact of an increasing Aerosol Optical Depth in the 300-2500 nm region.

3.6 Surface albedo

Not all incident solar irradiance that makes it through the absorption and scattering in the atmosphere gets absorbed by the earth. A portion of the radiation impinging on the surface of the earth gets reflected back, either out into space or into clouds where additional scattering and absorption can occur contributing to increased diffuse irradiation. The ratio between the reflected and incident irradiance is called the surface *albedo* [11]. The reflective properties of the earth's terrain are, just like with any other material, wavelength dependent and surface *albedo* can therefore be defined at any one number of spectral regions or as a function of wavelength. In this study, for sake of simplicity, *broadband surface albedo* is used to describe the varying reflective properties of the earth. *Broadband surface albedo* is defined as the ratio between impinging and reflected radiation across the shortwave spectral domain [37], which ranges from $400-3000\,nm$, in other words practically covers the entire spectral region of interest of this study. To determine the seasonal variations in *broadband surface albedo* around Visby during 2011 data from the *European Space Agency* project *GlobAlbedo* was used where various satellites sensors are combined to create surface *albedo* data for the entire globe [38]. The measured data consists of mean values across the shortwave domain measured during eight day periods and can be seen in Figure 16.

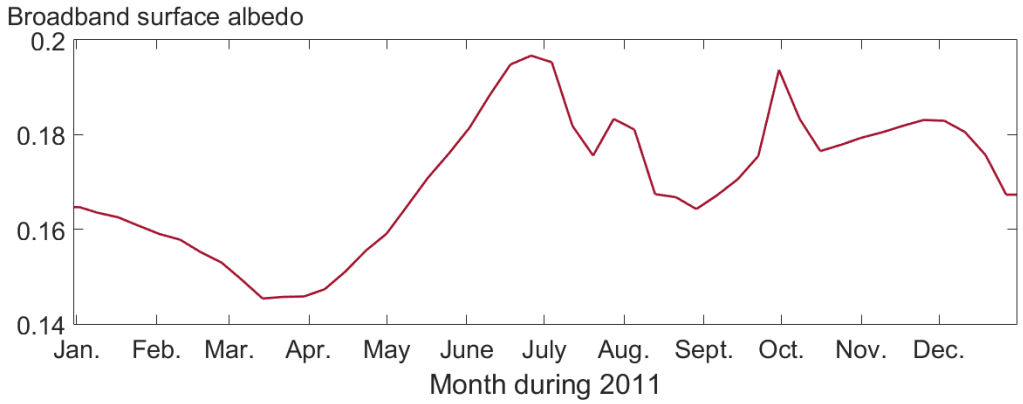

Figure 16. Broadband surface albedo variation of the Visby region during 2011. Data from [39].

Considering that areas covered in snow or ice generally have high *albedo* values [11] it may seem a bit contradictory that the measured *albedo* data for a relatively northern location such as Visby experiences a maximum *albedo* during summer and not in winter. According to Dr. Aku Riihelä, researcher at the *Finnish meteorological institute, FMI*, satellite measurements of surface *albedo* rely on available solar illumination on the site being measured and requires a solar *elevation angle* larger than 20 degrees to function reliably. During winter months at northern latitudes there is therefore a fair amount of uncertainty in the *albedo* measurements which could potentially explain the counterintuitive seasonal behavior seen in Figure 16 and the data during the winter months should perhaps therefore not be trusted blindly. Moreover it can be difficult to intuitively predict how a broadband surface *albedo* will behave since it is based on reflections of many wavelengths that are outside a humans visible range, materials we perceive as being highly reflective, for example snow, doesn't necessarily have to have a high reflectance outside of the visible range. Figure 17 shows the reflectance of three different types of vegetation as a function of the wavelengths used to determine a broadband surface *albedo*.

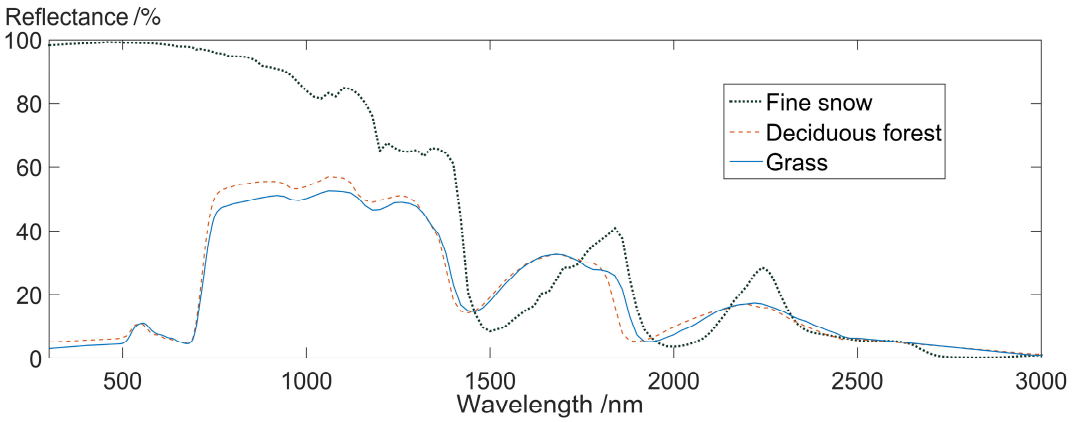

Figure 17. Reflectance as a function of wavelength for three types of vegetation. Data from [40].

3.7 Cloud parameters

Clouds, mists and other water droplet based formations are very common in the atmosphere and they play a big role in regulating the amount of solar irradiance reaching earth by limiting the atmospheric transparency and reflecting light back into space [41]. It's very complicated to model radiative transfer through the three-dimensional characteristics of clouds [4], many *radiative transfer models* including *SMARTS*, the *radiative transfer model* used to generate the *ASMT G173-03* reference spectrum, only model so-called *clear sky irradiance*, meaning that they treat the sky as cloudless, not taking clouds into consideration at all when modeling the spectra. *SBDART* on the other hand is capable of modelling spectrums under *all sky conditions,* which is the main reason why it was chosen as *radiative transfer model* for this study. To estimate the influence clouds have on a spectra *SBDART* requires information about the altitude, optical thickness and droplet size of the clouds.

The *cloud optical thickness* is defined as, similarly as in the case of *AOD*, the vertical integration of an *extinction coefficient* [42]. The *cloud extinction coefficient* is related to the product of the concentration and surface area of particles within a cloud [41]. Just like the name implies, the bigger the *cloud optical thickness* is the thicker a cloud appears to be, optically for incident light, not necessarily in terms of absolute geometric thickness. As can be seen illustrated in Figure 18, an increase in *cloud optical thickness* impacts the spectra in its entirety, predominantly in terms of *broadband irradiance*.

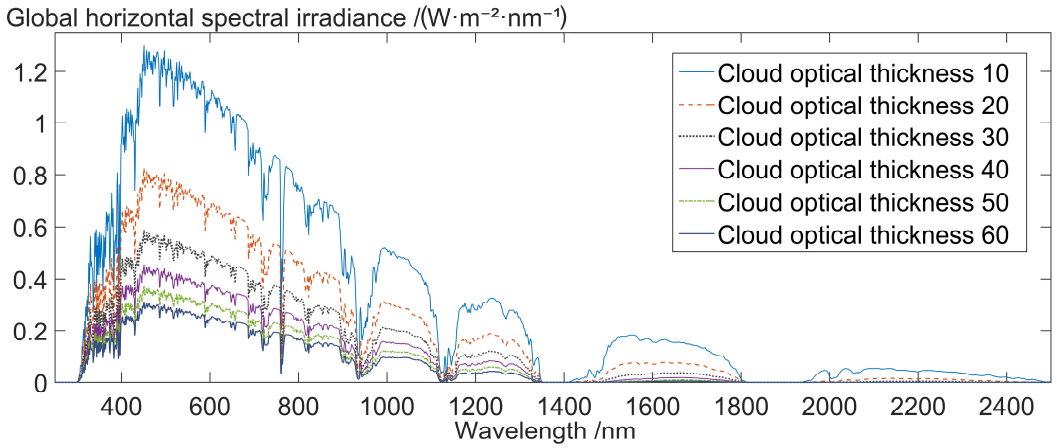

Figure 18. Simulated spectral effects of varying cloud optical thicknesses in the 300-2500 nm region.

The second cloud parameter, the cloud droplet radius, also known as cloud effective radius, is defined as a weighted mean value of the droplet radiuses within a cloud [43]. Mathematically it is expressed as shown in equation 7:

$$r_{eff} = \frac{\int_{r_1}^{r_2} \pi \cdot r^3 \cdot n(r)\, dr}{\int_{r_1}^{r_2} \pi \cdot r^2 \cdot n(r)\, dr} \quad (\mu\text{m}) \tag{7}$$

where $n(r)$ is the number of particles per unit volume with radius between r and $r + dr$, and the integration limits r_1 and r_2 represents the smallest and largest particle radius in the size distribution [44]. As can be seen in Figure 19, showing the *SBDART* simulated results of various *cloud droplet radiuses*, a small droplet radius weakens the spectral irradiance more than a large one in the visual part of the spectrum, but moving further into the near infrared region of the spectrum the opposite becomes true.

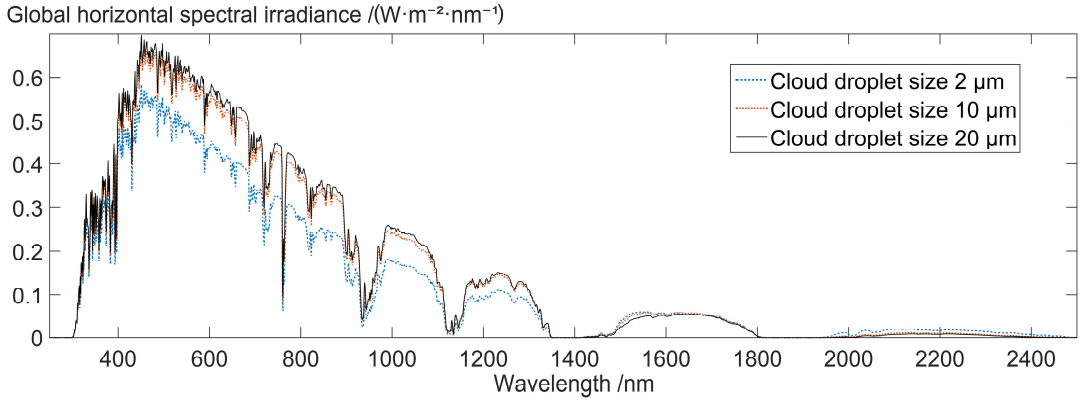

Figure 19. Simulated spectral effects of different cloud effective radiuses in the 300-2500 nm region.

The third cloud parameter used as input in the *radiative transfer model*, the *cloud top altitude,* also known as *cloud top height*, is probably the most straight forward parameter to understand. It is simply a measurement of the distance in meters between the earth and the highest level in the atmosphere where cloud properties are detectable [45]. The effects this property has on the shape of a spectrum in the $250 - 2500\ nm$ region appears, according to a parametric sweep of the property conducted in *SBDART*, to be virtually non-existing. According to the simulations it does however impact the irradiance at longer wavelengths. Figure 20 shows the simulated effects of an increasing *cloud top altitude* in parts of the mid-infrared region.

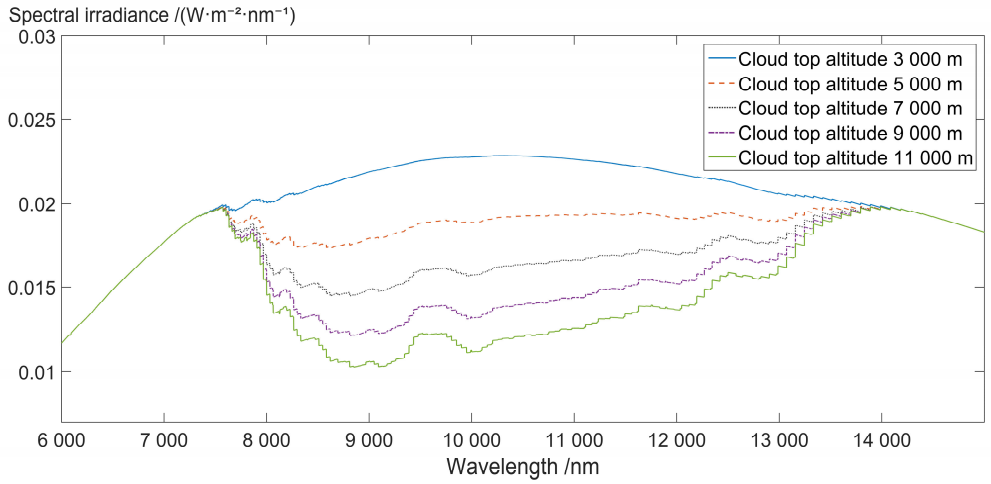

Figure 20. Spectral effects of cloud top height in the spectral region 6-14 microns.

Since the effects of a varying *cloud top height* are of a neglectable nature concerning the wavelength region of interest in this study, it was only used as an input parameter to the *radiative transfer model* because it was part of the same satellite dataset used to gather information about *cloud effective radius* and *cloud optical thickness* and required little additional effort to collect. It should be noted that *SBDART* also is capable of considering the *cloud bottom altitude* when defining clouds, but since a simulated parametric sweep of this property showed that the spatial thickness of clouds are of insignificant importance in the $280 - 2500\ nm$ region as long as the thickness of clouds already is described optically through the *cloud optical thickness*, which depends on the moisture density and vertical thickness of the cloud, the *cloud bottom altitude* property was excluded from the study and all clouds were assumed to have a constant spatial thickness of $1\ km$.

Variations in the three used cloud parameters, *cloud optical thickness, cloud effective radius* and *cloud top height* during 2011 were measured by the *Moderate-resolution Imaging Spectroradiometer*, *MODIS*, instrument onboard *NASA's Aqua* satellite. The data for all three cloud parameters were obtained as daily mean values and their variation during 2011 over Visby can be seen in Figure 21.

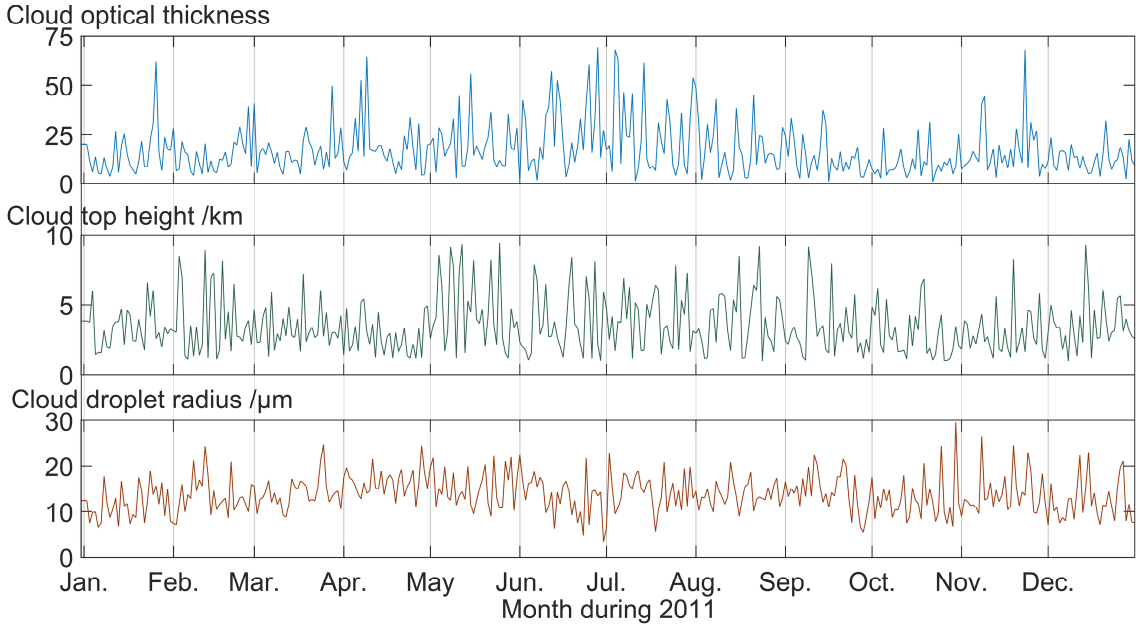

Figure 21. Daily variation of cloud optical thickness, cloud top height and cloud droplet radius over Visby during 2011. Data from [46].

Since the measured cloud parameters are daily values, using them as input for every simulated minute of the corresponding day would be like assuming that the sky is always to some extent covered by clouds, which would be just as unrealistic as not taking them into consideration at all. At *SMHI's* weather station in Visby every minute of a day is individually assigned a *clear-sky flag,* which according to Thomas Carlund, meteorologist at *SMHI*, is an assessment of the *atmospheric turbidity* and *optical aerosol depth* that is used to indicate if the measurements during a specific minute were disrupted by the presence of clouds or not. The *clear-sky flag* only assumes the values 1, indicating a cloud-free sky, or 0, indicating clouds in front of the

measuring instruments. When running the *SBDART* simulation on every minute during 2011, the simulation was set up to first read the *clear-sky flag* of the current time step, and then based on its value decide whether to use the daily cloud parameters in the simulation or completely bypass them and treat the sky as cloud-free. Since clouds can come and go within a matter of minutes many times each day this approach should provide a more dynamic and realistic behavior in the simulated spectral daily variations.

4 Spectral effects on PV-panels

4.1 Spectral response

Solar cells come in a variety of different materials that to some degree all have different physical properties. The properties that determines how capable a photovoltaic material is of generating electric current from an incident monochromatic light of a specific wavelength are the thickness of the cell and the size of the *band gap* [7], which is defined as the energy difference between the *valence band* and the *conduction band* in a semiconductor. In this study the spectral performance of the following eight materials will be evaluated; *Amorphous silicon* (*a-Si*), *Cadmium Telluride (CdTe), Gallium Arsenide (GaAs), Gallium Indium Phosphide (GaInP)*, *Monocrystalline Silicon (mono-Si), Multicrystalline Silicon (multi-Si), Copper Indium Gallium Selenide with Zinc Oxide (ZnO/CIGS)* and *Inorganic and Nanostructured Photovoltaics (InP).*

The *spectral response* is defined as the ratio between the generated current and incident light power, it describes how well a material can utilize light of a specific wavelength to generate electric current. The *spectral response* of the materials in this study was measured by the *National Renewable Energy Laboratory*, *NREL*, and can be seen in Figure 22 together with a normalized *ASTM G173-03* spectrum added for illustrational purposes. It is worth noticing that both *mono-Si* and *ZnO/CIGS* despite their wider spectral range have their peaks in spectral responsivity directly on top of one of the larger water vapour absorption regions in the terrestrial solar spectra.

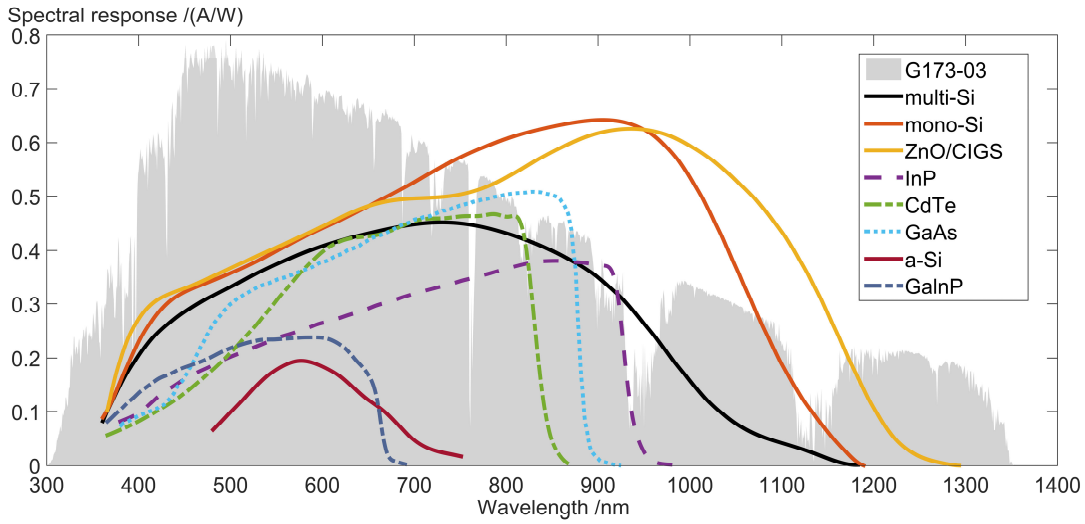

Figure 22. Spectral response of PV materials in the 300-1400 nm region. Data from [47].

4.2 Spectral Mismatch Factor

Photovoltaic modules are usually performance rated under *Standard Test Conditions* which incorporates the standard $AM1.5$ spectra [7]. To quantify how dissimilarities between the wavelength distribution of the reference spectra and the solar spectra incident on a PV-module

on a specific site effects the power output of the module, a parameter called *spectral mismatch factor, SMMF*, is used. The *spectral mismatch factor* uses the reference spectra, incident spectra, spectral response of the PV-module being tested and the spectral response of a reference device in order to determine if the incident spectral conditions are more or less favorable for the PV-module to generate current compared to the reference scenario. If the *SMMF* is precisely one it would mean that, as far as the tested PV-material is concerned, the incident spectra is exactly as well suited for current generation as the reference spectra. If the *SMMF* is less than one it would mean that the mismatch in spectral distribution between the reference spectra and incident spectra is such that it is unfavorable for the PV-material compared to how it was measured during *STC*. A *SMMF* value above one on the other hand would indicate the opposite – the incident spectra is more favorable for generating current compared to the reference conditions. The *spectral mismatch factor* is mathematically defined as [9]:

$$SMMF = \frac{\int_a^b E_{ref}(\lambda)\cdot S_r(\lambda)\,\mathrm{d}\lambda}{\int_a^b E_{inc}(\lambda)\cdot S_r(\lambda)\,\mathrm{d}\lambda} \cdot \frac{\int_c^d E_{inc}(\lambda)\cdot S_t(\lambda)\,\mathrm{d}\lambda}{\int_c^d E_{ref}(\lambda)\cdot S_t(\lambda)\,\mathrm{d}\lambda} \tag{8}$$

where λ is wavelength, $S_r(\lambda)$ is the spectral response of a reference device, $S_t(\lambda)$ is the spectral response of the device being tested, $E_{ref}(\lambda)$ is the spectral irradiance during reference conditions and $E_{inc}(\lambda)$ is the spectral irradiance on device being tested. The integration limits a, b and d, c represents the spectral range of the reference device and tested device respectively. The reference device is typically the instrument that was used to measure the irradiance on the site of interest, in this study the *broadband irradiance* was measured at *SMHI's* weather station using the *Kipp & Zonen CH1* pyrheliometer for direct irradiation and the *Kipp & Zonen CM21* pyranometer for diffuse irradiation. According to *Kipp & Zonens* instrument documentation, the *CM21* pyranometer is capable of measuring irradiance in the $305 - 2800\ nm$ range while the *CH1* is sensitive to wavelengths as low as $200\ nm$. But since the ASTM *G173-03* reference spectra is only defined down to wavelengths of $280\ nm$ [5] and wavelengths above $2500\ nm$ were not taken into consideration in the *radiative transfer model*, the integration limits for both cases in this study were set to $280 - 2500\ nm$.

According to Thomas Carlund at *SMHI* the transmission through the irradiation measuring devices occurs almost completely evenly at all measured wavelengths, practically giving them a constant *spectral response* of 1 over the whole spectral range. This means that equation 8 describing the *SMMF* for one specific material type and irradiance situation in this case can be written as:

$$SMMF = \frac{\int_{280}^{2500} E_{ref-G173}(\lambda)\,\mathrm{d}\lambda}{\int_{280}^{2500} E_{inc-SBDART}(\lambda)\,\mathrm{d}\lambda} \cdot \frac{\int_{280}^{2500} E_{inc-SBDART}(\lambda)\cdot S_{t-PVmaterial}(\lambda)\,\mathrm{d}\lambda}{\int_{280}^{2500} E_{ref-G173}(\lambda)\cdot S_{t-PVmaterial}(\lambda)\,\mathrm{d}\lambda} \tag{9}$$

The *spectral mismatch factor* can in combination with a measured *broadband irradiance* be used to define a *weighted irradiance* [7], which is expressed in watts per square meter like conventional *broadband irradiance*, but accounts for the effects of any spectral divergence between the reference spectra and incident spectra. Mathematically the *weighted irradiance* is expressed as the product of *SMMF* and *broadband irradiance*:

$$G_W = G_{BB} \cdot SMMF \quad (\mathrm{W \cdot m^{-2}}) \tag{10}$$

where G_{BB} is the *broadband irradiance* incident on a PV-module and $SMMF$ is the *spectral mismatch factor* for the same module and irradiation situation. Since both the *broadband irradiance* incident on a surface and its *SMMF* changes depending on surface tilt and azimuthal orientation, and since the *SMMF* is material specific, the *weighted irradiance,* G_W, needs to be determined for every combination of tilt, azimuth and material that one wishes to evaluate.

5 Solar angles and calculation of weighted irradiance

5.1 Irradiance on a tilted surface

The total solar irradiance reaching a tilted surface typically consists of three components: *direct irradiance,* G_b*, diffuse irradiance,* G_d*,* and *ground reflected irradiance,* G_g*,* which can be seen illustrated with their corresponding notation in Figure 23.

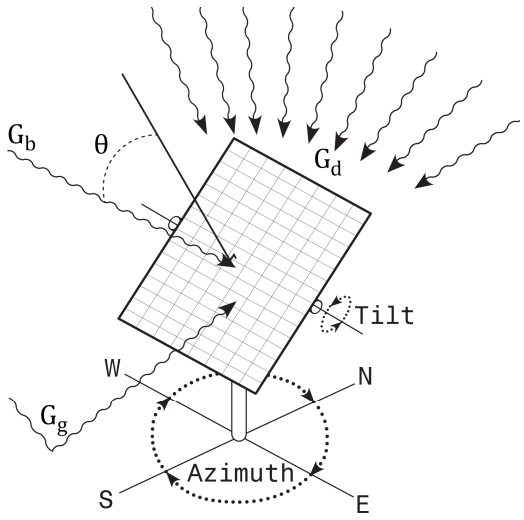

Figure 23. Illustration of the main parameters involved in solar angle calculations

The *direct irradiance,* also known as *beamed irradiance* is the solar irradiation reaching a surface directly from the same direction as the sun. It can be estimated as the irradiation striking a surface normal to the sun multiplied with the cosine of the incidence angle:

$$G_b = G_{b,n} \cdot \cos(\theta) \quad (\mathrm{W \cdot m^{-2}}) \tag{11}$$

where $G_{b,n}$ is the direct irradiance normal to the direction of the sun and θ is the incidence angle. In turn, the incidence angle depends on *solar altitude*, *solar azimuth*, surface tilt and surface azimuth as shown in equation 12:

$$\theta = \arccos(\cos(\alpha_s) \cdot \sin(\beta) \cdot \cos(\gamma_s - \gamma) \cdot \cos(\beta)) \quad (°) \tag{12}$$

where α_s represents the solar altitude, γ_s the solar azimuth, β the surface tilt and γ the surface azimuth.

The *diffuse irradiance* can be modeled in several different ways, in this study the *diffuse irradiance* is assumed to follow the simplest model available which is the isotropic model. In the isotropic model the *diffuse irradiance* is assumed to come down on a surface equally

distributed from across the entire sky dome. The amount of *diffuse irradiance* reaching a tilted surface compared to a horizontal surface then depends on the surface tilt according to:

$$G_d = G_{d,h} \cdot (1+\cos(\beta))/2 \quad (\mathrm{W \cdot m^{-2}}) \tag{13}$$

where $G_{d,h}$ is the diffuse irradiance on a horizontal surface and β is the surface tilt.

While the direct and diffuse components are purely geometrical descriptions modeled as if the surface in question was separated from any type of surroundings, the *ground reflected irradiance* requires the recognition of one surrounding surface with an embedded physical property, namely the reflectance of the ground. For *broadband irradiance* the *ground reflected irradiance* is defined as:

$$G_g = \rho_g \cdot G_h \cdot (1-\cos(\beta))/2 \quad (\mathrm{W \cdot m^{-2}}) \tag{14}$$

where ρ_g is the broadband reflectance of the ground, G_h is the *global horizontal irradiance* and β is the surface tilt. It can however be considered too approximate to use a broadband average to describe the reflective properties of the ground [48] and when dealing with spectrally resolved irradiance one might as well acknowledge that the reflectance of whatever surface the PV-module is located on probably isn't spectrally uniform, and the *ground reflected irradiance* can therefore be defined as a function of wavelength:

$$G_g(\lambda) = \rho_g(\lambda) \cdot G_h(\lambda) \cdot (1-\cos(\beta))/2 \quad (\mathrm{W \cdot m^{-2} \cdot nm^{-1}}) \tag{15}$$

In the calculations carried out in this study the ground was considered to be covered in grass, which was chosen as to be representative of a variety of circumstances such as the green roof of a building in an urban scenario or someone's garden in a rural setting. The reflective properties of this grass as a function of wavelength can be seen in Figure 17. In calculations involving ground reflectance of broadband irradiance using equation 14 the mean value of the grass reflectance in Figure 16 was used as ρ_g.

The total irradiation reaching a tilted surface at any given time and orientation can then be determined by the summation of the direct, diffuse and ground reflected irradiation components:

$$G_{Total\,\mathrm{tilted}}(\lambda) = G_b(\lambda) + G_d(\lambda) + G_g(\lambda) \quad (\mathrm{W \cdot m^{-2} \cdot nm^{-1}}) \tag{16}$$

5.2 Calculation sequence

To obtain the *weighted irradiance* for all combinations of surface tilt and azimuth during a year in Visby needed to assess what the optimal tracking direction is, the first step of the calculation sequence is to calculate the *zenith angle,* which directly determines how long the *atmospheric length* will be. The *zenith angle* will depend on location and time and can be

calculated as 90 degrees subtracted by the *solar altitude* where the *solar altitude* is determined by equation 17:

$$\alpha_s = \arcsin(cos(\delta) \cdot cos(\omega) \cdot cos(\lambda) + sin(\delta) \cdot sin(\lambda)) \quad (°) \tag{17}$$

where δ represents the *declination angle* of the earth, ω is the *hour angle* and λ is the latitude of the site.

With a *zenith angle* assigned for every minute during 2011 the *radiative transfer model SBDART* was run for each minute with a *zenith angle* smaller than 89.9° together with the corresponding atmospheric data presented in chapter 3 for each time step to generate *global horizontal* and *direct horizontal* incident solar spectrums. The corresponding *diffuse horizontal* irradiance for each time step can then easily be obtained as the difference between the two:

$$G_{d,h}(\lambda) = G_h(\lambda) - G_{b,h}(\lambda) \quad (\mathrm{W \cdot m^{-2} \cdot nm^{-1}}) \tag{18}$$

where $G_h(\lambda)$ and $G_{b,h}(\lambda)$ are the global and direct horizontal irradiances with respect to wavelength. By using the equations described in chapter 5.1 the three types of horizontal irradiances were then recalculated to represent the irradiation that would reach a surface at any time, tilt and azimuth during 2011.

When this is done an estimation of the spectral distribution of the incident irradiation reaching a surface will be attained, but to ensure a realistic outcome it is important that the amplitude of the modelled spectra is adjusted so that it matches the *broadband irradiance* measured on site [10]. The *broadband irradiance* measured at the weather station is therefore also recalculated using the formulas described in chapter 5.1 so that a surface for each minute and orientation combination that could have occurred in Visby during 2011 has two types of tilted irradiations assigned to it – a spectrally resolved irradiation and a *broadband irradiation*. The amplitude adjustment of the spectrally resolved irradiation is then calculated by:

$$G_{adj}(\lambda) = G_{SBDART}(\lambda) \cdot \frac{G_{SMHI}}{\int_{280}^{2500} G_{SBDART}(\lambda)} \quad (\mathrm{W \cdot m^{-2} \cdot nm^{-1}}) \tag{19}$$

where G_{SBDART} is the tilted simulated spectrally resolved irradiance and G_{SMHI} is the tilted *broadband irradiance*.

The spectrally resolved irradiation on a tilted surface can then be combined with the spectral response of the specific material and the $AM1.5$ reference spectra to calculate the *spectral mismatch factor* for every combination of minute, material, tilt and azimuth that could have occurred during 2011. In combination with total tilted *broadband irradiance* this will then finally produce the *weighted irradiance* of the surface. If every possible combination were to be assessed with a one degree resolution there would be $1440(minute) \cdot 365(day) \cdot 181(tilt) \cdot 360(azimuth) \cdot 8(material)$ number of possible *spectral mismatch factors* that could occur during a year. To exhaust all of these possibilities is a time consuming task even

with today's modern computers. Therefore, to reduce the computation time required, the calculations carried out within this study were limited to only considering surface azimuth with a two degrees incremental resolution, thereby reducing the number of possible *SMMF*'s to a manageable $1.37 \cdot 10^{11}$ different annual combinations. A flowchart illustrating the described calculation sequence that was used in this study to obtain the *weighted irradiance* can be seen in Figure 24.

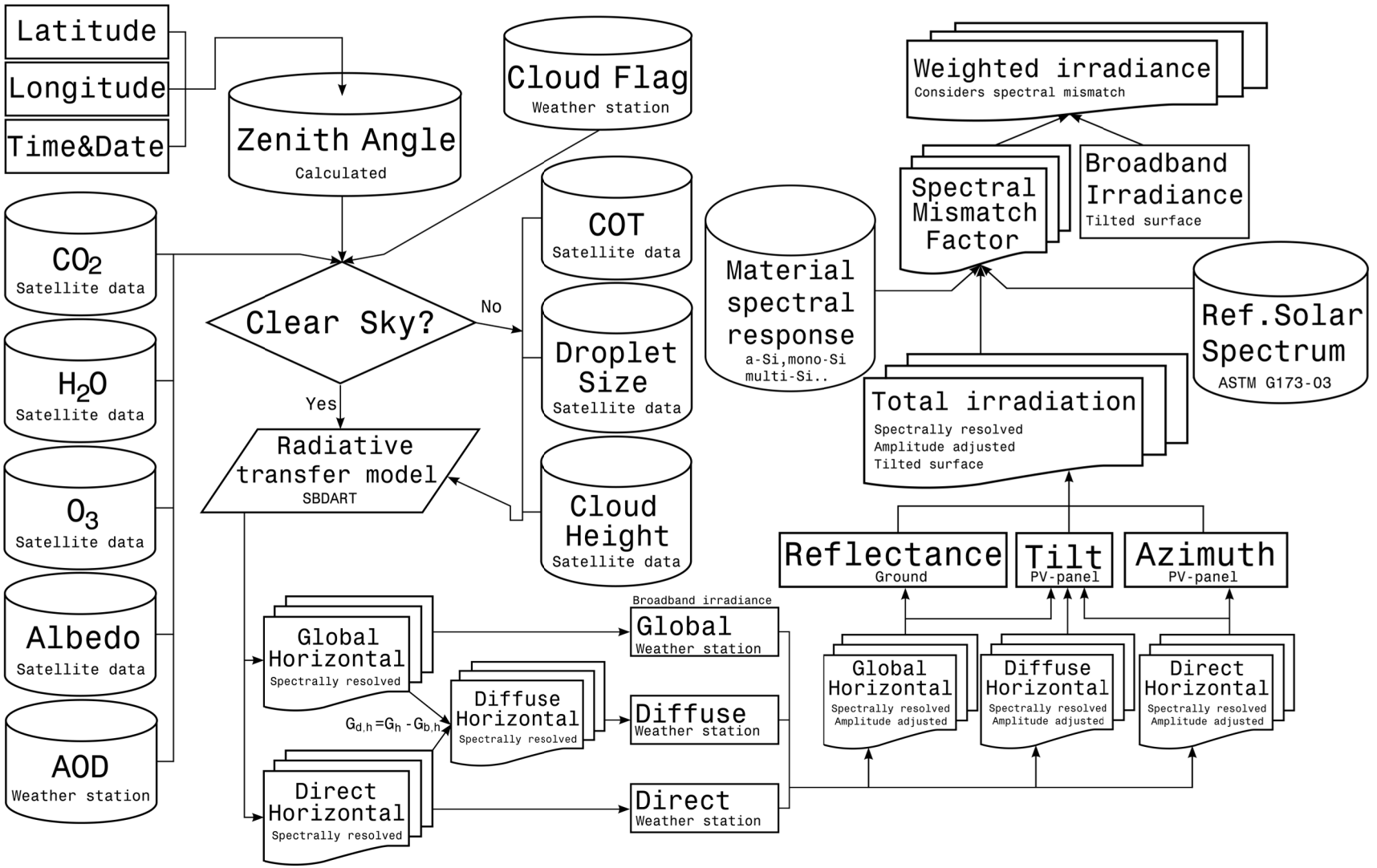

Figure 24. Flow chart of calculation sequence used to obtain weighted irradiance.

6 Simulation results

6.1 Modelled irradiation

Figure 25 shows the *SBDART* simulated solar spectrums for a horizontal surface before amplitude adjustment compared to the *SMHI* measured *broadband irradiation* for the same surface on the 7th January. Like many other days of the year in Sweden 7th of January 2011 was a partially overcast day where direct sunlight was almost entirely filtered out during several hours of the day. This is why the irradiance in Figure 25 appears to have two separate predominant characteristics during the day – one part with almost exclusively diffuse irradiation and another part consisting of both direct and diffuse components.

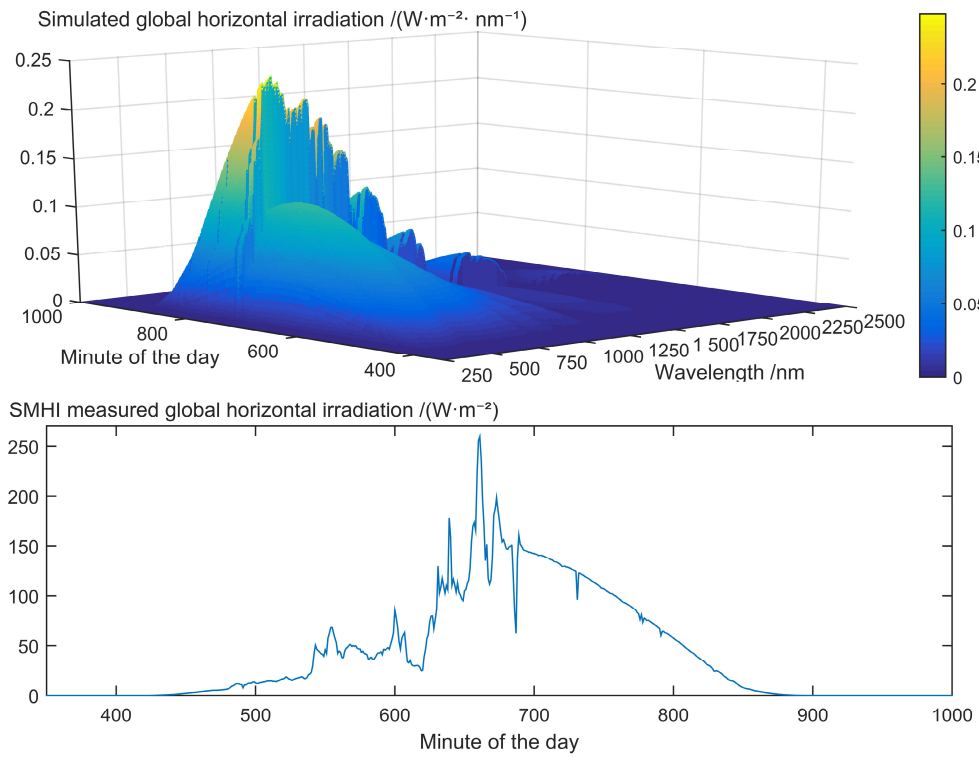

Figure 25. SBDART simulated global spectral irradiance (top) and SMHI measured broadband irradiance (bottom) for a horizontal surface on the 7th January 2011 in Visby.

The unprocessed *SBDART* simulated radiation shown in Figure 25 does a reasonable job at depicting the main characteristics of the irradiation during the 7th January because of the *clear-sky flags* indicating the presence of clouds to the simulation. However, the simulation does not manage to reproduce all the minor irradiation fluctuations during the day, one explanation for this could be that the simulations cloud input data is based on measured daily mean values of cloud properties and in reality the *cloud optical thickness* and other cloud properties could contain rapid variations during the course of a day that are not accounted for in the simulation. This is why the amplitude adjustment of the modelled spectra is crucial in terms adding realism to the irradiation. Figure 26 shows the same modelled spectrums of 7th January as in

Figure 25 but after the amplitude adjustment process has taken place. In Figure 26 the integrated intensity of the spectra of each minute precisely matches the *broadband irradiance* measured by *SMHI*, this results in much more dynamic and realistic spectrum intensity variations. By comparing the spectral irradiance values seen in Figure 25 and Figure 26 it can also be seen that the unprocessed modelled spectra fails to capture the quickly emerging irradiation maxima occurring around mid-day, making the maximum irradiation value of the unprocessed spectra significantly lower compared to the *SMHI* measured values, which is yet another indication that amplitude adjustment of the irradiation on a minute by minute basis is necessary.

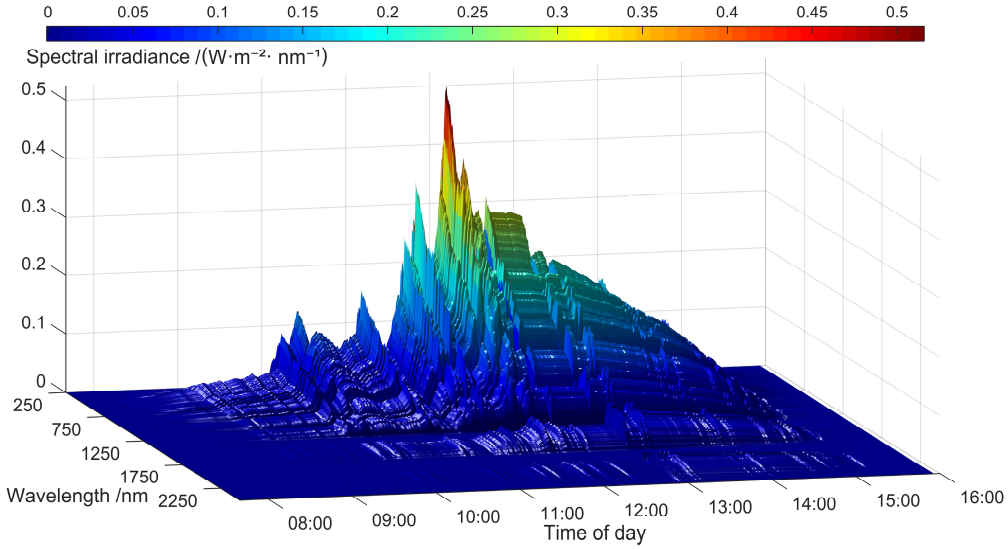

Figure 26. Simulated amplitude adjusted solar spectrums for a surface with 0° tilt during 7th January 2011 in Visby.

6.2 Spectral mismatch

6.2.1 Spectral mismatch as a function of panel tilt

The calculated variations in *spectral mismatch factor* indicates that in terms of panel tilt there are two main categories of materials with different physical characteristics within the eight studied PV materials. One category consisting of *Inorganic and Nanostructured Photovoltaics (InP), Monocrystalline Silicon (mono-Si),* and *Copper Indium Gallium Selenide with Zinc Oxide (ZnO/CIGS).* And a second category including *Multicrystalline Silicon (multi-Si), Amorphous silicon (a-Si), Cadmium Telluride (CdTe), Gallium Arsenide (GaAs),* and *Gallium Indium Phosphide (GaInP).* The results implies that the first mentioned category generally will have an increasing *spectral mismatch factor* along with an increasing tilt of the panel. For the second mentioned category the opposite is true – the *spectral mismatch factor* decreases with increasing panel tilt. A possible reason behind this is that *ZnO/CIGS* and *mono-Si*, which have a broader spectral response compared to the other materials in the study, are favored by the spectral reflective properties of the grass used in this study. If a different material than grass would have been used to describe the ground reflective properties, the *spectral mismatch factor* for all materials could potentially look very different at high surface tilts. It should also be emphasized that a high *spectral mismatch factor* doesn't necessarily

indicate a good panel orientation, it is the combination of *broadband irradiance* and *spectral mismatch factor* together with the modules efficiency that determines what the electricity production of any orientation will be. Figure 27 illustrates the simulated typical characteristic shapes of *spectral mismatch factor* as a function of surface tilt and time of day for two types of materials representative of the two main material categories previously mentioned.

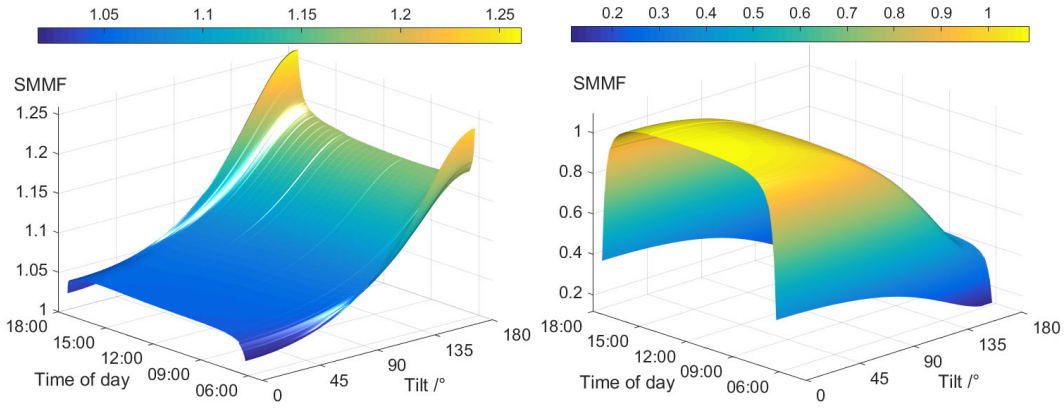

Figure 27. Typical daily behavior of simulated SMMF as a function of tilt and time of day for mono-Si (left) and a-Si (right). Calculated for south facing module orientations at 4th of March 2011.

6.2.2 Cloud effects on spectral mismatch

During many of the simulated days the shape of the daily *spectral mismatch factor* curve does not look as even and theoretically perfect as it appears in Figure 27. The basic shape of a material, as seen in Figure 27, can be distinguished during every day of the year, but very often there are times during a day when the characteristic curve gets interrupted and the *spectral mismatch factor* changes rapidly. The only atmospheric variable capable of inducing spectral changes that arise and disappear within a matter of minutes are clouds. Figure 28 shows the simulated *spectral mismatch factor* of a *CdTe* module with 57° tilt facing south on the 15th February 2011 together with light blue shaded areas indicating the occurrence of active *cloud flags* from *SMHI's* weather station.

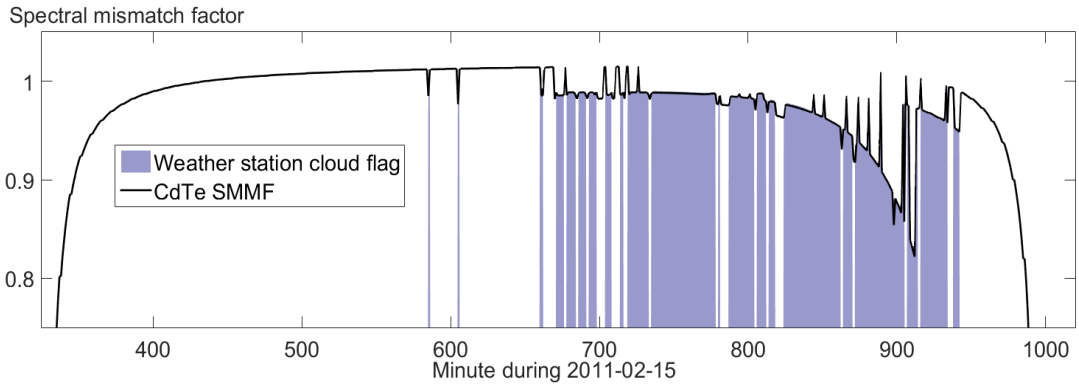

Figure 28. Correlation between spectral mismatch factor abnormality and presence of clouds for a CdTe module with 57° tilt facing south on the 15th February.

As can be seen in Figure 28 the presence of clouds has a negative impact on the *spectral mismatch factor,* which is not only the case for *CdTe,* but for all the studied PV materials. This means that effects clouds have on PV electricity production is probably even more devastating in reality than what a calculation based on only *broadband irradiance* would suggest, because if a cloud causes the *spectral mismatch factor* to go below one, the *broadband irradiance,* the intensity of which is already weakened by clouds covering the sky, will be multiplied with a value less than one when generating the *weighted irradiance* and therefore the weighted intensity of the irradiation becomes even further reduced.

6.2.3 SMMF as a function of season and tracking strategy

As can be seen in Figure 22 there is a big variety in the spectral responsiveness of the eight studied materials. Some materials, like *Copper Indium Gallium Selenide with Zinc Oxide, ZnO/CIGS,* are sensitive to a wide range of wavelengths and are able to generate current from light all the way up to 1300 *nm* in the infrared region. Other materials, such as *Gallium Indium Phosphide, GaInP,* only operates within parts of the visual range. Because weather and atmospheric conditions exhibit seasonal variations that effects the spectral distribution of terrestrial solar radiation it is therefore not unlikely that certain materials finds parts of the annual spectral distribution cycle more favorable than others. Additionally, as illustrated in Figure 27, the *spectral mismatch factor* of a material can change significantly with surface tilt, so the final *SMMF* of a panel will depend on solar position, atmospheric conditions, surface orientation and material type. Figure 29 shows the simulated results of daily mean *spectral mismatch factor* for each of the eight materials when following a conventional 2-axis tracking strategy that continuously orients the panel so that it minimizes the incidence angle between the panel and the sun.

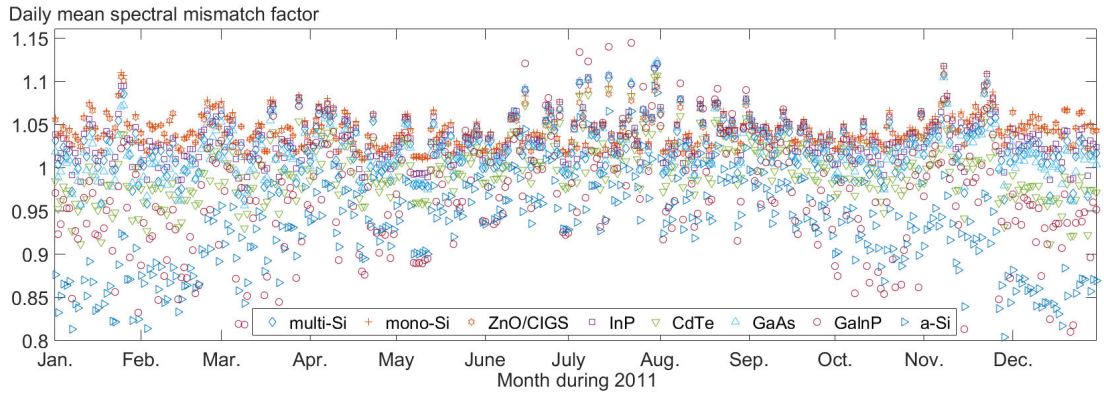

Figure 29. Daily mean spectral mismatch factor for each of the eight materials when tracking the minimum incidence angle.

As can be seen in Figure 29, the angle of incidence minimizing tracking strategy induces a big spread in *SMMF* among the materials. Especially interesting is the fact that some materials appears to be highly spectrally unfavored during big parts of the winter months. The likely explanation behind this phenomena is that the solar *elevation angle* in Sweden is very low during these parts of the year, and consequently, to minimize the angle of incidence the tracking system needs to use very high surface tilts and in doing so it is in essence forcing the panels away from the diffuse irradiation, which very well could be the main source of

irradiation at the time, and down towards the ground reflected irradiation. Depending on the optical properties of the ground, certain materials can spectrally be negatively affected by this while other materials remain unaffected or potentially even benefit from it. The results shown in Figure 29 could indicate that the performance and suitability of a tracking strategy is interconnected with the choice of PV material and geographical location, and in the case of a conventional angle of incidence minimizing tracking system in Scandinavia - *GaInP* and *a-Si* could be bad material choices. The PV materials that appears to generate the highest spectral gains with the angle of incidence minimizing tracking system are the two with the broadest spectral response range – *mono-Si* and *ZnO/CIGS*.

The resulting daily mean *SMMF* of a tracking system that instead of following a predefined path, continuously identifies the direction at which the highest *weighted irradiance* occurs and positions a panel perpendicular to it can be seen in Figure 30. As can be seen in Figure 30, this strategy produces a narrower *SMMF* spread across the materials compared to a conventional tracking strategy. The most striking difference between the two strategies is the effects seen on *Gallium Indium Phosphide,* which went from being among the most spectrally unfavored materials when using a conventional tracking system, to often being the most spectrally favored material when using a *weighted irradiance* tracking system. The reason for why *GaInP* and *a-Si* appears to benefit more than other materials from the change in tracking strategy could be because they have a narrower spectral response which could make them more vulnerable to spectral changes while materials like *ZnO/CIGS* and *mono-Si,* which have wider response curves, remains more stable and unaffected towards irradiation changes.

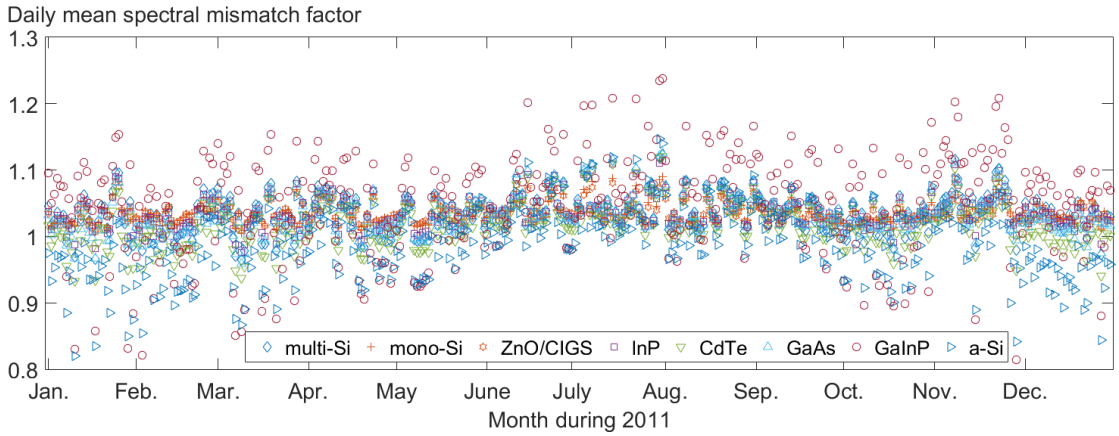

Figure 30. Daily mean spectral mismatch factor for each of the eight materials when tracking the maximum weighted irradiation.

6.3 What on earth should we track?

One of the main advantages of a conventional tracking system that seeks to minimize the angle of incidence between a panel and the beamed irradiation is that for each time step the upcoming tilt/azimuth combinations required for tracking are perfectly predicable. And since both future and past combinations can be calculated it is easy to already in the design stage of a device establish the positioning limits which the tracking system must be able to handle. Figure 31 shows all the necessary tilt/azimuth combinations required to position a surface perpendicular to the direct irradiation direction during every minute of 2011 in Visby. As can

be seen in Figure 31, it is not necessary for a tracking system that strives to minimize the incidence angle to be able to position itself all the way from $0 - 180°$ tilt since only values in the range of about $35 - 150°$ occurs. It should also be noted that the combinations shown in Figure 31 includes time steps after sunset, so when confining the tracking to times when the *solar elevation angle* is greater than 0° the tilt and azimuth range that needs to be covered on an annual basis becomes even smaller.

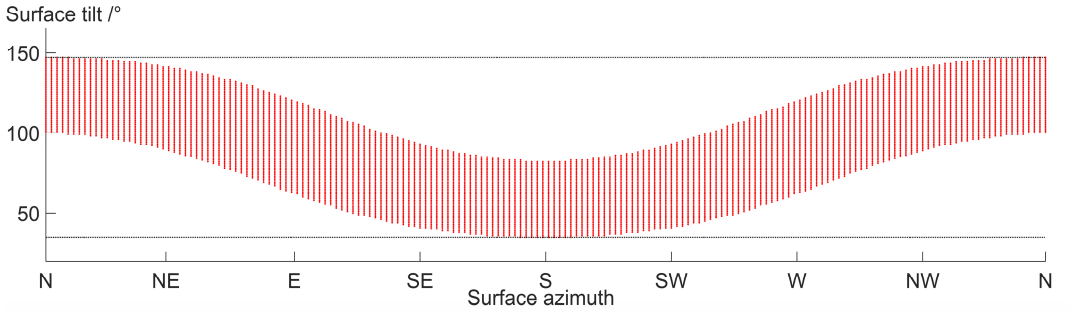

Figure 31. Combinations of tilt/azimuth needed to orient a surface in a way that minimizes the angle of incidence for every minute during 2011 in Visby.

A tracking strategy that instead during every individual minute of a day manages to identify the theoretically optimal panel tilt/azimuth combination based on *weighted irradiance* can however behave much more chaotic and unpredictable. Figure 32 shows the tilt/azimuth combinations that should be chosen to minimize the angle of incidence during 21th June compared to the combinations where the highest *weighted irradiance* values were simulated to occur. The tilt/azimuth combinations chosen by the angle of incidence minimizing tracking strategy follows the path of the sun and starts towards the northeast and moves towards the northwest in a predictable way during a day. The position in which the maximum *weighted irradiance* occurs can however move back and forth in azimuthal orientation several times a day, to clarify in the illustration when during the course of the day each tilt/azimuth combination corresponds to the *weighted irradiance* tracking points in Figure 32 have been color coded with a gradient so that a bluer color represents a maximum *weighted irradiance* occurring early in the day and a more yellow color corresponds to a combination occurring later in the day. It should also be noted that several points in Figure 32 can have the same color nuance, this is because when tracking *weighted irradiance,* some time steps contains more than one optimal tracking position. This is also always the case when 0° tilt is chosen, at that point all azimuth orientations will receive an equal amount of irradiation and they can all be considered optimal.

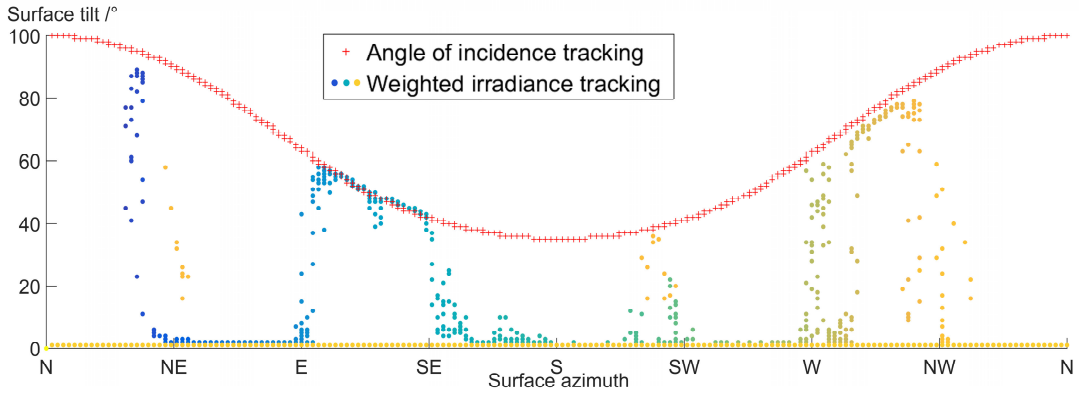

Figure 32. Tilt and azimuth combinations that minimizes the angle of incidence during a day compared to the combinations that were simulated to theoretically generate the most electricity for a multi-Si PV panel during 21th June 2011.

As can be seen from Figure 32 the tilt/azimuth combination that receives the most *weighted irradiance* during the 21th June is more often than not different from the combination suggested by the angle of incidence minimizing tracking strategy. This can be seen as an indication that the diffuse irradiation component during the 21th June must have been intense enough to compete with the irradiation that would have been received on a surface pointed directly towards the sun. The more predominant the direct irradiation is during a day, the more similar the two tracking strategies becomes. As can be seen in Figure 33, showing the two tracking strategies during the 3rd of August which was a sunnier day, the maximum *weighted irradiance* very often occurs directly on top of the angle on incidence tracking points, indicating a predominant direct irradiation component.

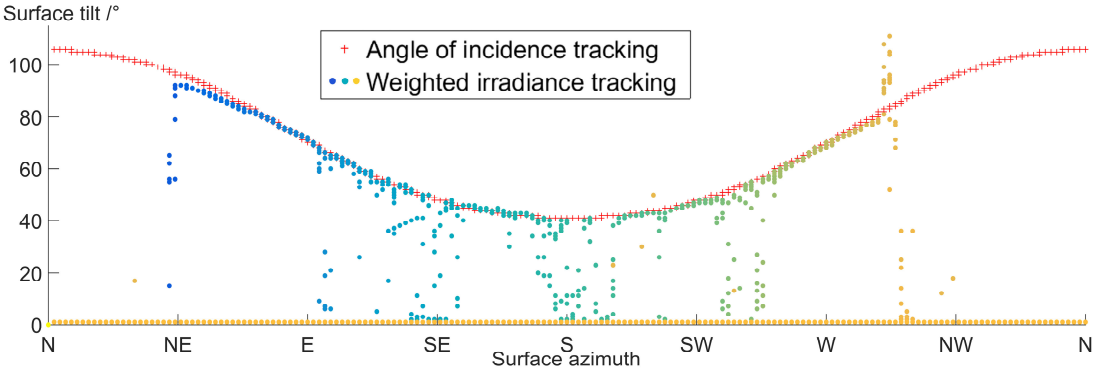

Figure 33. Tilt and azimuth combinations that minimizes the angle of incidence during the day compared to the combinations that could theoretically generate the most electricity for a multi-Si PV panel during 3rd August 2011.

It can also be seen in Figure 32 and Figure 33 that the maximum *weighted irradiance* often occurs somewhere in between the minimum angle of incidence and 0° surface tilt, which means that the direction from which the most electricity could be generated from, often is acquired by creating a tilt/azimuth combination that compromises between diffuse, direct and ground reflected irradiation. In rare cases the optimum tilt can also briefly be seen positioned above the minimum angle of incidence, which indicates that during these time steps a large part of the *weighted irradiance* is likely coming from ground reflected irradiation.

Since the *SMMF* is individual for each material, the direction at which the maximum *weighted irradiance* occurs doesn't necessarily have to be the same for each PV material. Figure 34 shows the tilt/azimuth combinations where the maximum *weighted irradiance* was simulated to take place for all eight studied materials during the 3rd of August, a day with predominant direct irradiation.

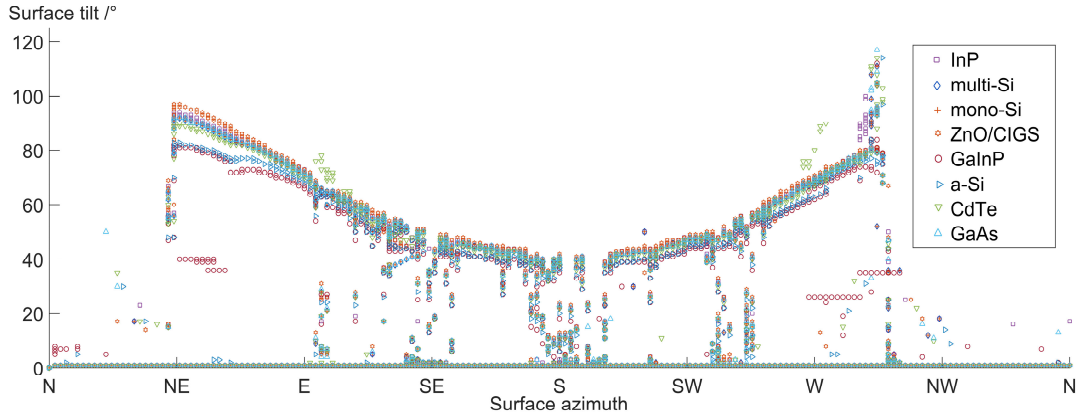

Figure 34. Tilt and azimuth combinations that maximizes the weighted irradiance for each of the eight materials during each minute of the 3rd of August 2011.

As can be seen in Figure 34 there is a certain disagreement among the materials as to where the maximum *weighted irradiance* occurs and some materials, such as *GaInP,* are spectrally benefitted from choosing a surface tilt a few degrees lower compared to other materials. However, overall the materials in Figure 34 appears to be drawn to a common underlying shape, a shape which approximately corresponds to where the minimum incidence angle would be positioned if marked in the figure. Figure 35 shows the position at which maximum *weighted irradiance* occurs during the 10th October, which was a significantly cloudier day with a predominant diffuse irradiation component, together with the positions at which minimal incidence angle occurs.

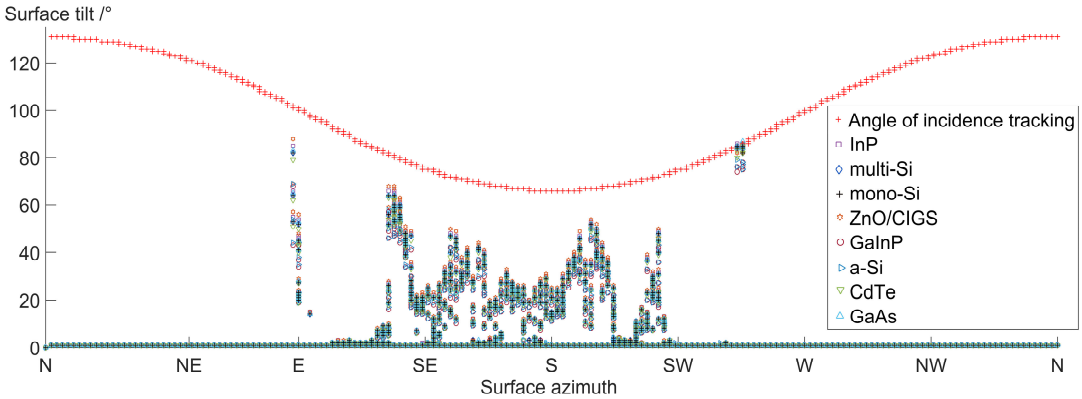

Figure 35. Tilt and azimuth combinations that maximizes the weighted irradiance for each of the eight materials during each minute of the 10th of October 2011 together with the combinations that would minimize the incidence angle.

As can be seen in Figure 35, during the 10th of October there appeared to be very little correlation between the points which minimized the incidence angle and the tilt/azimuth combinations where maximum *weighted irradiance* occurred. While this gives the impression that tracking the minimum incidence angle was a horrible idea during the 10th of October in Visby, Figure 35 only indicates that the *weighted irradiance* is higher in certain tilt/azimuth combinations different from a panel orientation orthogonal to the suns direction, it does not quantify by how much. It is quite possible that the difference in received *weighted irradiance* when following the angle of incidence minimizing tracking strategy compared to a *weighted irradiance* tracking strategy often is small enough to be considered neglectable, even at times when the received irradiance is not theoretically maximal using the conventional system.

Figure 36 shows the simulated daily accumulated *weighted irradiance* received per square meter of *CdTe* for the two different tracking strategies, both in an ideal 2-axis situation and when confined to tracking along a single axis. The 1-axial tracking strategies confined to tilt tracking have been assigned to face south and the 1-axial azimuth tracking is assumed to have a fixed surface tilt equal to the site latitude.

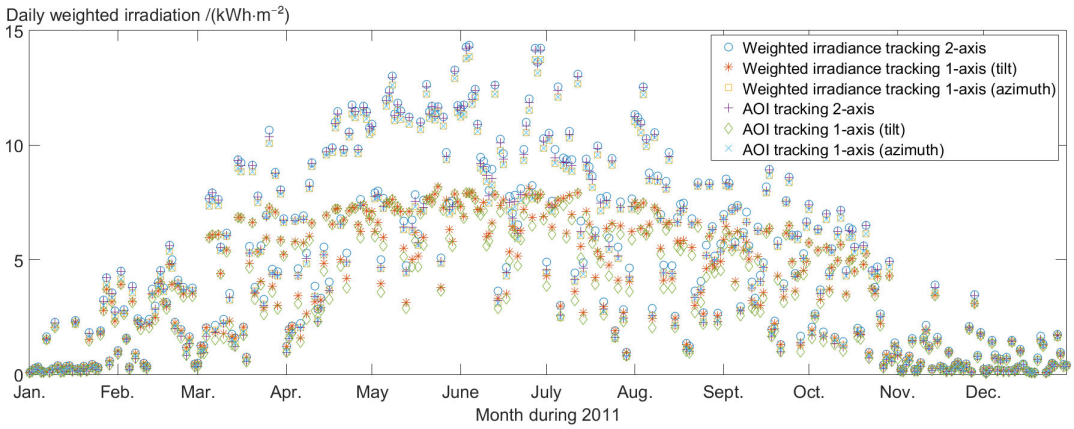

Figure 36. Daily weighted irradiation received by a Cadmium Telluride module following different tracking strategies.

As seen in Figure 36, the angle of incidence minimizing tracking strategy constantly performs worse than a strategy that identifies the maximum *weighted irradiance*. The difference between the two strategies however, does not appear to be very big. It can also be seen from Figure 36 that regardless of whether an angle of incidence minimizing strategy or a maximum *weighted irradiance* strategy is implemented, in a single axial tracking system, tracking along the azimuthal direction with a fixed tilt appears to be more productive than vice versa.

Figure 37 shows the different received *weighted irradiances* by various materials, all continuously oriented to capture the maximum amount of *weighted irradiance*. It should be emphasized that the exact tilt/azimuth combinations required by each material to obtain the maximum *weighted irradiance* is to some degree individual, which was previously shown in Figure 34 and Figure 35, so the chosen tilt/azimuth combinations required to obtain the results shown in Figure 37 is unique for each material.

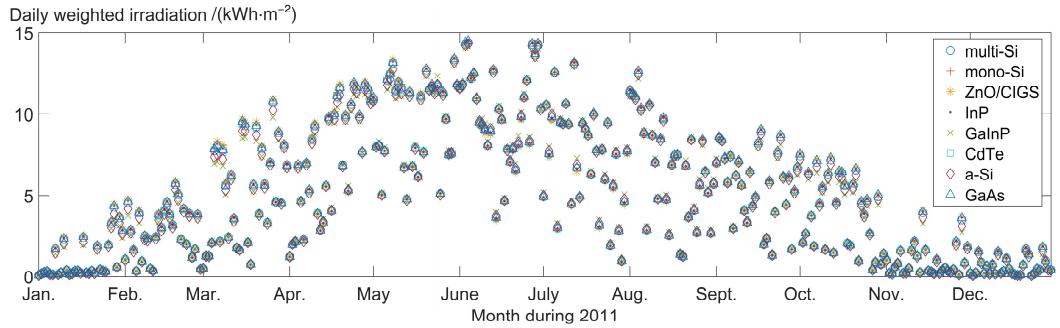

Figure 37. Daily weighted irradiation received on different materials tracking the optimal weighted irradiance point during every minute of the year.

In general, the maximum *weighted irradiance* that can be accumulated during each day of the year appears to be roughly the same for all eight materials and the irradiances differ only within a few percent from each other.

The actual electricity output that can be yielded from a PV module is determined by a multiplication of its incident *weighted irradiance* and the efficiency of its cells. In reality the cell efficiency is not entirely constant but changes with temperature, soiling, aging etc. For sake of simplicity these variations are not accounted for in this study and a constant cell efficiency, measured under *STC*, is used to approximate the annual energy production. Table 1 shows the measured cell efficiencies of all the eight materials in this study.

Table 1. Confirmed module efficiencies measured under STC with the ASTM G-173-03 spectra. Data from [49].

GaAs	*CdTe*	*ZnO/CIGS*	*InP*	*a-Si*	*Mono-Si*	*Multi-Si*	*GaInP*
24.1%	16.1%	19.8%	22.1%	10.1%	25.0%	20.4%	37.9%

As seen in Table 1, an average PV cell efficiency tends to lie in the region of about 20%, meaning that 20% of the incident power will be converted to electricity. *Gallium Indium Phosphide* however sticks out with a significantly higher cell efficiency. Because of its high efficiency, *GaInP* is often used to generate electricity on satellites in space and in similar situations that demand high performance [50], and the material could potentially be considered too luxurious for most residential applications.

Figure 38 shows the calculated cumulative electricity production per square meter for each of the eight materials during 2011 based on the corresponding cell efficiencies seen in Table 1, both when applying a conventional angle of incidence minimizing tracking strategy and a tracking strategy that finds the maximum *weighted irradiance*.

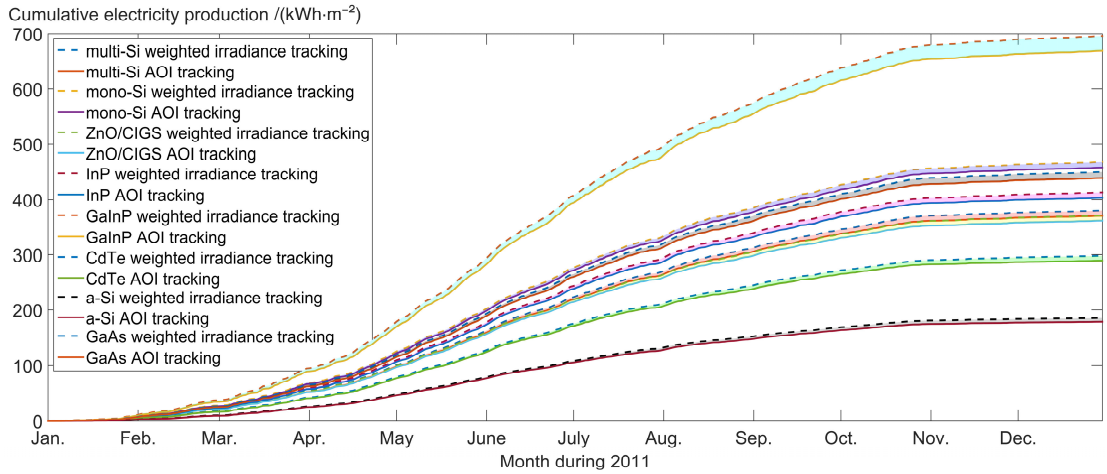

Figure 38. Cumulative electricity production during 2011 for the eight studied materials for both maximum weighted irradiance tracking strategy and minimum angle of incidence tracking.

The shaded areas in Figure 38 represents the discrepancy in energy production between the two tracking strategies for each material, or in other words, how much energy the conventional angle of incidence minimizing strategy is failing to produce compared to an optimal *weighted irradiance* tracking strategy. The discrepancies between the strategies can be explained by a combination of annual *spectral mismatch factor* variation and incident *broadband irradiance* variation. As previously seen in Figure 29, *Gallium Indium Phosphide (GaInP),* is one of the materials that suffers the biggest *SMMF* losses while following an angle of incidence minimizing tracking strategy. This is, in combination with the materials high efficiency, probably why *GaInP* is the material that could benefit the most from a *weighted irradiance* maximizing tracking system compared to a conventional tracking strategy. As can be seen in Figure 38, most PV materials would be able to annually generate around ten kilowatt hours of electricity more per square meter by following a *weighted irradiance* tracking system compared to an angle of incidence minimizing system. Figure 39 illustrates more clearly how big the annual production difference is between the two strategies and how much the annual energy yield in theory could be increased by tracking the optimal *weighted irradiance*.

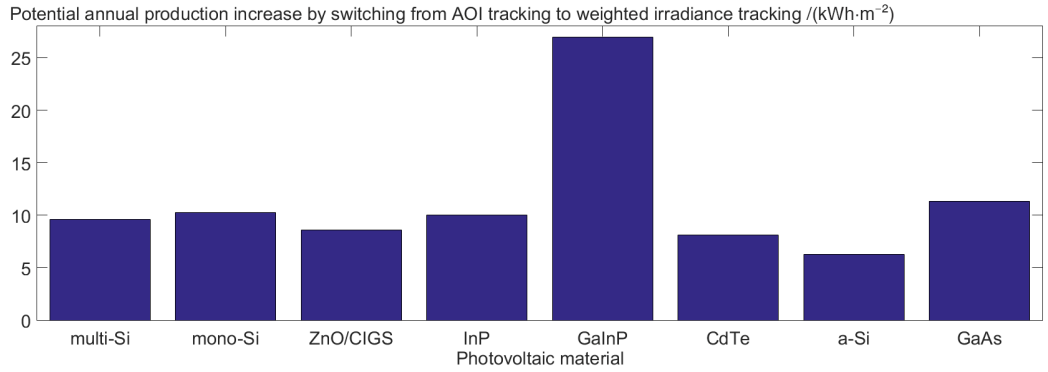

Figure 39. Calculated annual energy production increase when switching from a 2-axis angle of incidence minimizing tracking system to a 2-axis weighted irradiance maximizing system in Visby.

7 Conclusions & discussion

In none of the simulated days during 2011 were all the tilt/azimuth combinations yielding the highest *weighted irradiance* the same as they would have been in an angle of incidence minimizing tracking system. Which in a way answers the initial question which was if we should point our PV panels in a Nordic climate where the sun doesn't shine or not – We should! Because the *weighted irradiance* in a Scandinavian climate is often higher there.

The main challenge in doing so lies in continuously identifying where the highest *weighted irradiance* occurs. It could hypothetically be possible to do this without involving any type of irradiation sensors by continuously monitoring the available satellite and weather station measured atmospheric compounds and use a machine learning approach to try and predict what the atmospheric weather situation will be like in upcoming time steps and then run a *radiative transfer model* with the predicted atmospheric data as input before the situation takes place in reality and position the tracking device according to where the maximum *weighted irradiance* is anticipated to occur. This strategy has probably never been implemented before and its accuracy and feasibility could therefore be regarded as uncertain, especially since clouds can come and go within minutes or seconds which makes them very problematic to predict. An easier and probably more reliable approach would be to physically measure the radiation around the tracking device in real time using light sensors. But even this approach has its inherent challenges since light intensity measuring sensors, for example photo resistors, have their own imbedded spectral response properties that could be very different from that of the PV panel used with the tracking device which thereby makes the irradiation readings biased. A way around this could be to have light sensors made of the exact same material as the PV module installed on the tracking device, essentially smaller versions of the bigger PV panel mounted in the tracking system, to measure the irradiation and decide where the system should be pointed. This way both the spectral response of the PV material and the wavelength distribution of the incident sunlight will be accounted for and what the sensors are outputting should in essence be *weighted irradiation*, without the need of any adjustment calculations. A problem with this approach is that it would require a lot of sensors to be aligned in a spherical configuration in order to register the full radiation situation surrounding the tracking device, which would potentially be costly.

Furthermore the results of this study indicates that if the direction at which maximum *weighted irradiance* occurs could continuously be determined, tracking the *weighted irradiance* may require more violent and frequent direction changes compared to a conventional tracking system. If this is the case there is a possibility that the energy required by the tracking systems mechanical parts to carry out the direction changes outweigh the energy that could potentially be generated with the new panel orientation. So that even if a certain module direction would be able to generate more electricity in theory, the net increase in productivity could be smaller than the results of this study suggests or even negative.

The results of *SMMF* as a function of surface tilt indicates that there are certain PV materials that could be better suited for high tilts, meaning that they receive more radiation from ground reflectance, and other materials that due to their optical properties could be more suitable for low or horizontal tilts. In this study the spectral reflectance properties of the ground were assumed to follow the grass curve seen in Figure 17, if the reflective properties of the ground

would change it is possible that the categories of materials preferring high/low tilts could change completely and the assessment of how to orient a panel is probably therefore best done on a project specific basis.

The results of the study also showed that *spectral mismatch factor* to some degree depends on tracking strategy. The results indicates that materials with a narrow spectral response, such as *a-Si* and *GaInP*, are spectrally unfavored by the conventional angle of incidence minimizing tracking strategy in Visby and would benefit the most from a *weighted irradiance* tracking strategy. The results also indicates that the sunnier a climate is, the closer to being optimal the angle of incidence minimizing strategy appears to be. This could mean that if a *weighted irradiance* maximizing tracking device would be implemented in reality, climates with weak direct irradiation relative to the diffuse and ground reflected components could be considered favorable candidates. Hypothetical examples of places where this should be the case could for instance be highly polluted cities in Asia, that in theory should receive a lot of direct irradiation due to their geographical circumstances, but where the inhabitants finds it appropriate to generate a dense layer of lethal smog covering the atmosphere above their city and thereby filters out a lot of the direct irradiation. In such locations it could be difficult to predict which direction the maximum irradiance is coming from and a *weighted irradiance* maximizing tracking system could potentially perform particularly well. Another example could be arctic climates where the landscape is covered in snow during large parts of the year, making the reflective properties of the ground such that the ground reflected irradiation can contend with the intensity of the direct and diffuse components. Yet another example could be in an urban environment where reflections, both specular and diffuse, off of a multitude of manmade materials both change the spectral distribution of the incident sunlight and creates spots with higher or lower concentrations of energy compared to what would could be found in an unobstructed area.

7.1 Future research

In this study the naturally occurring irradiation conditions of an unshaded grass surface during 2011 in Visby were assessed and the results indicates that by knowing how the spectral irradiance surrounding a PV module behaves, it should be possible to increase the electricity production by tracking the maximum *weighted irradiance*. However, accepting the spectral irradiance reaching a site as it is when it arrives and then chase the direction of maximum spectral benefit might not be the most efficient approach. Instead, if one would change the environment of a PV module array, based on the PV materials spectral response curve, by surrounding it with materials that have spectral reflective properties that maximizes the reflection at desired wavelengths while minimizing at others, it should be possible to generate *spectral mismatch factors* far higher than what can be found occurring naturally. Not only would this be able to increase the *spectral mismatch factor*, filtering out the correct wavelengths before reflecting irradiation onto a PV panel should also enable the design of concentrating PV systems that doesn't heat up as much as regular designs. For example, *Epsomite*, which is a white mineral substance which can be found on for instance cave walls in Spain, has a spectral reflectance that can exceed 80% in the range where the spectral responsiveness of many PV materials is the highest, and at the same time its reflectance drops

drastically around 1400 nm where many PV materials cease to be responsive which can be seen in Figure 40.

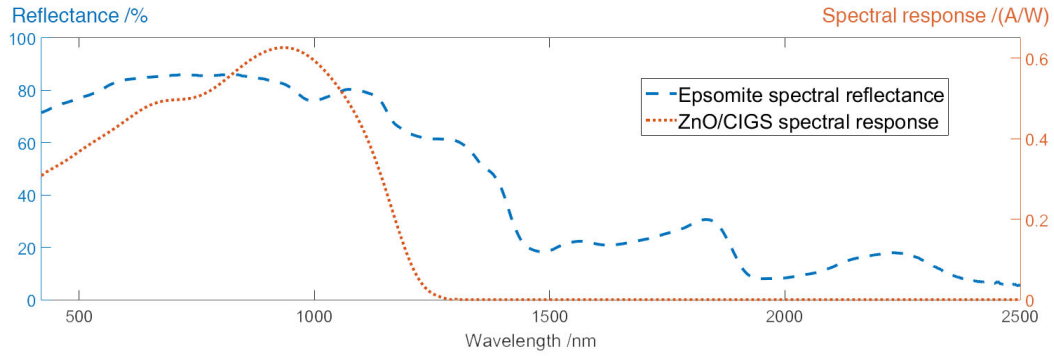

Figure 40. Spectral reflectance of Epsomite together with the spectral response curve of ZnO/CIGS.

This means that if one were to for example construct a parabolic shaped wall coated in a material like *Epsomite* and position a PV module in front of it, without having to move the PV module at all, it should be possible to expose the module to a wavelength distribution almost perfectly matching that which the cell is responsive to, and at the same time filter away unwanted wavelengths so that the cell is kept cooler than it otherwise would and thereby the cell efficiency is increased and the final electricity production becomes absolutely colossal. In short; spectrally engineering an environment so that its reflections matches the responsiveness of a PV material is such an ingenious idea that it probably has the potential to change the world and it is something that every university immediately needs to recognize as an important field of research.

7.2 Limitations

According to Thomas Carlund, meteorologist at *SMHI,* the *clear-sky flag* determined each minute at the Visby weather station, which was used in this study to indicate to the *radiative transfer model* if the sky was cloudy or not, only considers the cloud situation directly in front of the measuring instruments. This means that situations such as when a small cloud appears in front of the measuring instruments, but the rest of the sky is cloud-free, is not realistically taken into consideration in the simulation, instead one small cloud has the potential to render the whole sky cloudy. Even though the amplitude adjustment of the spectra makes sure that the total irradiance amount is correct, depicting the cloud situation in such a binary way, where either the entire sky is cloudy or cloud-free, could for example over- or underestimate the diffuse irradiation during some time steps. The fact that weather stations rarely measures spectrally resolved solar irradiance is also a limitation since it makes it difficult to compare the simulated spectral irradiance from a *radiative transfer model* with real world data to verify its accuracy.

Another limitation of the study is that only wavelengths up to 2500 nm were simulated, which was done to reduce the required simulation time, while ideally wavelengths of at least up to 2800 nm would have been needed to match the pyranometer limits of the weather station. The spectral intensity within the $2500 - 2800\ nm$ range is however low enough to

be considered neglectable, for instance, the integrated spectral intensity in the $2500 - 2800\ nm$ region of the *ASTM G173-03* reference spectra, which represents a bright and sunny day with radiation values higher than what can typically be seen in Sweden, is less that one watt per square meter.

References

[1] U.S. Department of Energy, 'Users Manual for TMY3 Data Sets', National Renewable Energy Laboratory, Battelle, 2008.

[2] Rredc.nrel.gov, 'RReDC Glossary of Solar Radiation Resource Terms'. [Online]. Available: http://rredc.nrel.gov/solar/glossary/gloss_b.html. [Accessed: 29- Apr- 2015].

[3] Ise.fraunhofer.de, 'STC Measurements — Fraunhofer ISE', 2015. [Online]. Available: http://www.ise.fraunhofer.de/en/service-units/callab-pv-cells-callab-pv-modules/callab-pv-modules/stc-measurements. [Accessed: 29- Apr- 2015].

[4] D. Myers, *Solar radiation*. Boca Raton: CRC Press/Taylor & Francis Group, 2013, pp. 67,127.

[5] 'Tables for Reference Solar Spectral Irradiances: Direct Normal and Hemispherical on 37 Tilted Surface', 2012.

[6] T. Behrendt, J. Kuehnert, A. Hammer, E. Lorenz, J. Betcke and D. Heinemann, 'Solar spectral irradiance derived from satellite data: A tool to improve thin film PV performance estimations?', *Solar Energy*, vol. 98, p. 100, 2013.

[7] T. Behrendt, J. Kühnert, A. Hammer, E. Lorenz, J. Betcke and D. Heinemann, 'Spectrally Resolved Solar Irradiance from Satellite Data to Investigate the Performance of Thin Film Photovoltaics', in *25th European Photovoltaic Solar Energy Conference and Exhibition / 5th World Conference on Photovoltaic Energy Conversion*, Valencia, Spain, 2010, pp. 492-494.

[8] P. Ricchiazzi, S. Yang, C. Gautier and D. Sowle, 'SBDART: A Research and Teaching Software Tool for Plane-Parallel Radiative Transfer in the Earth's Atmosphere', *Bulletin of the American Meteorological Society*, vol. 79, no. 10, pp. 2101-2114, 1998.

[9] B. Marion, 'Influence of Atmospheric Variations on Photovoltaic Performance and Modeling Their Effects for Days with Clear Skies', in *2012 IEEE Photovoltaic Specialists Conference*, 2012, p. 2.

[10] G. Litjens, 'Investigation of Spectral Effects on Photovoltaic Technologies by Modelling the Solar Spectral Distribution', MSc., University of Utrecht, 2013.

[11] U. Schumann, *Atmospheric Physics*. Berlin, Heidelberg: Springer Berlin Heidelberg, 2012, pp. 135-138,43, 37-38, 59,61, 17-18.

[12] I. Morison, *Introduction to astronomy and cosmology*. Chichester, U.K.: Wiley, 2008, pp. 46-47,50.

[13] S. Beeby and N. White, *Energy harvesting for autonomous systems*. Norwood, Mass.: Artech House, 2010, pp. 51-52.

[14] C21.phas.ubc.ca, 'Simple Earth Climate Model - Additional Concept Explanations | C21 Physics Teaching for the 21st Century', 2010. [Online]. Available: http://c21.phas.ubc.ca/article/simple-earth-climate-model-additional-concept-explanations. [Accessed: 10- Apr- 2015].

[15] International Astronomical Union, IAU, 'RESOLUTION B2 on the re-definition of the astronomical unit of length.', 2012.

[16] P. Ekholm, *Formler och tabeller i fysik, matematik och kemi*. Göteborg: Konvergenta, 1997.

[17] P. Altermatt, 'Measurement of the solar constant', *Pvlighthouse.com.au*. [Online]. Available: http://www.pvlighthouse.com.au/resources/courses/altermatt/The%20Solar%20Spectrum/Measurement%20of%20the%20solar%20constant.aspx. [Accessed: 13- May- 2015].

[18] C. Frohlich, 'Composite of daily solar irradiance', *PMOD/WRC, Davos, Switzerland, 2012.*, 2012. [Online]. Available: http://ftp.pmodwrc.ch/pub/data/irradiance/composite/DataPlots/composite_42_64_1502.dat. [Accessed: 10- Apr- 2015].

[19] G. Yordanov, O. Midtgård, T. Saetre, H. Nielsen and L. Norum, 'Overirradiance (Cloud Enhancement) Events at High Latitudes', *IEEE Journal of Photovoltaics*, vol. 3, no. 1, pp. 271-277, 2013.

[20] X. Yin, 'Optical air mass: Daily integration and its applications', *Meteorology and Atmospheric Physics*, vol. 63, no. 3-4, pp. 227-233, 1997.

[21] Pveducation.org, 'Terrestrial Solar Radiation | Air Mass'. [Online]. Available: http://www.pveducation.org/pvcdrom/properties-of-sunlight/air-mass#footnote1_85by44z. [Accessed: 13- May- 2015].

[22] Ozonewatch.gsfc.nasa.gov, 'Ozone Hole Watch: Facts about Dobson Units', 2013. [Online]. Available: http://ozonewatch.gsfc.nasa.gov/facts/dobson_SH.html. [Accessed: 10- Apr- 2015].

[23] Epa.gov, 'Ozone Science: The Facts Behind the Phaseout | Ozone Layer Protection |US EPA', 2010. [Online]. Available: http://www.epa.gov/ozone/science/sc_fact.html. [Accessed: 10- Apr- 2015].

[24] R. Goody and Y. Yung, *Atmospheric radiation*, 2nd ed. New York: Oxford University Press, 1989, pp. 207-208.

[25] Smhi.se, 'UV-strålning | SMHI', 2015. [Online]. Available: http://www.smhi.se/kunskapsbanken/meteorologi/uv-stralning-1.3849. [Accessed: 13- Apr- 2015].

[26] Temis.nl, 'TEMIS -- ToGoMi Total Ozone Column -- archive', 2015. [Online]. Available: http://www.temis.nl/protocols/o3col/o3col-omi.php?year=2011. [Accessed: 10- Apr- 2015].

[27] C. Helmis and P. Nastos, *Advances in meteorology, climatology and atmospheric physics*. Berlin: Springer, 2013, pp. 1026-1027.

[28] Disc.sci.gsfc.nasa.gov, 'DATA PRODUCTS V5 — GES DISC - Goddard Earth Sciences Data and Information Services Center', 2015. [Online]. Available: http://disc.sci.gsfc.nasa.gov/AIRS/data-holdings/by-data-product-v5. [Accessed: 10- Apr- 2015].

[29] Exelisvis.com, 'Fast Line-of-sight Atmospheric Analysis of Hypercubes (FLAASH) // Water Vapor Units', 2015. [Online]. Available: http://www.exelisvis.com/docs/FLAASH.html. [Accessed: 13- Apr- 2015].

[30] DWD: Germany, 'CM SAF // Product // Catalog // Vertically integrated water vapour', *Wui.cmsaf.eu*, 2014. [Online]. Available: https://wui.cmsaf.eu/safira/action/searchProdukt. [Accessed: 13- Apr- 2015].

[31] V. Ramanathan, and A. Vogelmann, 'Greenhouse Effect, Atmospheric Solar Absorption and the Earth's Radiation Budget: From the Arrhenius-Langley Era to the 1990s', *Ambio*, vol. 26, no. 1, p. 45, 1997.

[32] M. Chaplin, 'Water absorption spectrum', *Www1.lsbu.ac.uk*, 2015. [Online]. Available: http://www1.lsbu.ac.uk/water/water_vibrational_spectrum.html. [Accessed: 14- Apr- 2015].

[33] S. Kempler, 'Aerosol Optical Thickness — GES DISC - Goddard Earth Sciences Data and Information Services Center', *Disc.sci.gsfc.nasa.gov*, 2013. [Online]. Available: http://disc.sci.gsfc.nasa.gov/data-holdings/PIP/aerosol_optical_thickness_or_depth.shtml. [Accessed: 15- Apr- 2015].

[34] M. H.Bergin, 'Aerosol Radiative Properties and Their Impacts', in *From weather forecasting to exploring the solar system*, 1st ed., Les Ulls: EDP Sciences, 2010, pp. 1-2 Chapter 4.

[35] Smhi.se, 'Solstrålning | SMHI |Aerosoler och ozon', 2015. [Online]. Available: http://www.smhi.se/kunskapsbanken/meteorologi/solstralning-1.4186. [Accessed: 15- Apr- 2015].

[36] R. Bergstrom, P. Pilewskie, P. Russell, J. Redemann, T. Bond, P. Quinn and B. Sierau, 'Spectral absorption properties of atmospheric aerosols', *Atmos. Chem. Phys.*, vol. 7, no. 23, pp. 5937-5943, 2007.

[37] C. Barker Schaaf, 'Assessment of the status of the development of the standards for the Terrestrial Essential Climate Variables', UNFCCC, Rome, 2009.

[38] Ecmwf.int, 'ESA-GlobAlbedo | ECMWF', 2014. [Online]. Available: http://www.ecmwf.int/en/esa-globalbedo. [Accessed: 16- Apr- 2015].

[39] Globalbedo.org, 'globalbedo.org', 2015. [Online]. Available: http://www.globalbedo.org/get.php. [Accessed: 10- Apr- 2015].

[40] Speclib.jpl.nasa.gov, 'ASTER Spectral Library - Version 2.0 — Spectral Library'. [Online]. Available: http://speclib.jpl.nasa.gov/. [Accessed: 16- Apr- 2015].

[41] A. Kokhanovsky, 'Optical properties of terrestrial clouds', *Earth-Science Reviews*, vol. 64, no. 3-4, p. 14, 2004.

[42] Disc.sci.gsfc.nasa.gov, 'Cloud Optical Thickness — GES DISC - Goddard Earth Sciences Data and Information Services Center', 2009. [Online]. Available: http://disc.sci.gsfc.nasa.gov/giovanni/additional/data-holdings/PIP/cloud_optical_thickness_or_depth.shtml. [Accessed: 16- Apr- 2015].

[43] Disc.sci.gsfc.nasa.gov, 'Cloud Effective Radius — GES DISC - Goddard Earth Sciences Data and Information Services Center', 2009. [Online]. Available: http://disc.sci.gsfc.nasa.gov/data-holdings/PIP/cloud_effective_radius.shtml. [Accessed: 16- Apr- 2015].

[44] J. Hansen and L. Travis, 'Light scattering in planetary atmospheres', *Space Sci Rev*, vol. 16, no. 4, p. 548, 1974.

[45] Arm.gov, 'ARM - Measurement - Cloud top height'. [Online]. Available: https://www.arm.gov/measurements/cloudtopheight. [Accessed: 17- Apr- 2015].

[46] Ladsweb.nascom.nasa.gov, 'LAADS Web -- Search for Data Products', 2015. [Online]. Available: http://ladsweb.nascom.nasa.gov/data/search.html. [Accessed: 17- Apr- 2015].

[47] H. Field, 'Solar Cell Spectral Response Measurement Errors Related to Spectral Band Width and Chopped Light Waveform', in *26th IEEE Photovoltaic Specialists Conference*, Anaheim, California, 1997, p. 3.

[48] P. Altermatt, 'The reflectance of the ground', *Pvlighthouse.com.au*. [Online]. Available: http://www.pvlighthouse.com.au/resources/courses/altermatt/The%20Solar%20Spectrum/The%20reflectance%20of%20the%20ground.aspx. [Accessed: 22- Apr- 2015].

[49] M. Green, K. Emery, Y. Hishikawa, W. Warta and E. Dunlop, 'Solar cell efficiency tables (version 43)', *Progress in Photovoltaics: Research and Applications*, vol. 22, no. 1, pp. 1-9, 2013.

[50] F. Dimroth, C. Baur, A. Bett, M. Meusel and G. Strobl, '3-6 junction photovoltaic cells for space and terrestrial concentrator applications', *Conference Record of the Thirty-first IEEE Photovoltaic Specialists Conference, 2005.*, p. 525, 2005.

LUND UNIVERSITY

Dept of Architecture and Built Environment: Division of Energy and Building Design
Dept of Building and Environmental Technology: Divisions of Building Physics and Building Services